TR-0318

AN ANALYTIC PHASE FUNCTION FOR CYLINDRICAL PARTICLES

August 1992

Patti Gillespie

US ARMY
LABORATORY COMMAND
ATMOSPHERIC SCIENCES LABORATORY
White Sands Missile Range, NM 88002-5501

NOTICES

Disclaimers

The findings in this report are not to be construed as an official Department of the Army position, unless so designated by other authorized documents.

The citation of trade names and names of manufacturers in this report is not to be construed as official Government indorsement or approval of commercial products or services referenced herein.

Destruction Notice

When this document is no longer needed, destroy it by any method that will prevent disclosure of its contents or reconstruction of the document.

REPORT DOCUMENTATION PAGE

Form Approved
OMB No. 0704-0188

1. AGENCY USE ONLY (Leave blank)	2. REPORT DATE	3. REPORT TYPE AND DATES COVERED
	August 1992	Final

4. TITLE AND SUBTITLE

An Analytic Phase Function for Cylindrical Particles

5. FUNDING NUMBERS

TA: 62784/AH71/E

6. AUTHOR(S)

Patti Gillespie

7. PERFORMING ORGANIZATION NAME(S) AND ADDRESS(ES)

U.S. Army Atmospheric Sciences Laboratory
White Sands Missile Range, NM 88002-5501

8. PERFORMING ORGANIZATION REPORT NUMBER

ASL-TR-0318

9. SPONSORING/MONITORING AGENCY NAME(S) AND ADDRESS(ES)

U.S. Army Laboratory Command
Adelphi, MD 20783-1145

10. SPONSORING/MONITORING AGENCY REPORT NUMBER

11. SUPPLEMENTARY NOTES

12a. DISTRIBUTION/AVAILABILITY STATEMENT

Approved for public release; distribution is unlimited.

12b. DISTRIBUTION CODE

13. ABSTRACT *(Maximum 200 words)*

In this report an analytic phase function for cylindrical particles is developed based on considerations used to develop the Henyey-Greenstein phase function and functions based on electromagnetic theory calculations. The phase function developed in this report is compared to other phase functions and its usefulness is demonstrated. An annotated bibliography on the subject of phase functions for cylindrical particles is included.

14. SUBJECT TERMS

scattering, aerosol, cylindrical particles, radiative transfer, extinction.

15. NUMBER OF PAGES

46

16. PRICE CODE

17. SECURITY CLASSIFICATION OF REPORT	18. SECURITY CLASSIFICATION OF THIS PAGE	19. SECURITY CLASSIFICATION OF ABSTRACT	20. LIMITATION OF ABSTRACT
Unclassified	Unclassified	Unclassified	SAR

ACKNOWLEDGMENT

This work was originally performed when the author was employed at the Clinton P. Anderson Physical Science Laboratory at New Mexico State University under contract to the U.S. Army Atmospheric Sciences Laboratory. The subject matter of the report was suggested by Dr. Robert Sutherland who also suggested that this report be submitted as a technical report. The assistance of the many people involved in getting this report published, both previously at PSL and currently at ASL, is appreciated.

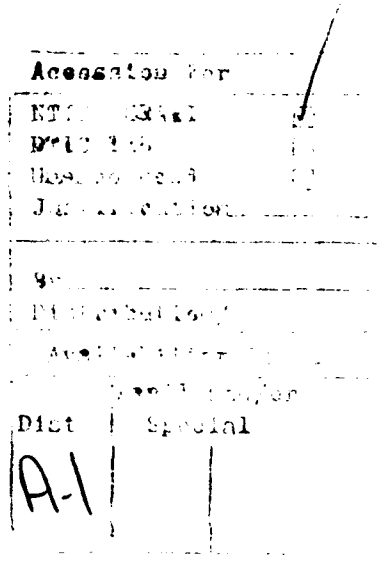

CONTENTS

LIST OF ILLUSTRATIONS

LIST OF TABLES

1. INTRODUCTION

This report discusses an analytic form for the phase function (scattering intensity pattern) for cylindrical particles in the visible wavelength region. Numerical phase functions exist for cylindrical particles, and these have been used to compare to experimental data (Bohren and Huffman, 1983). The goal is to show that by comparison to accepted numerical phase functions, a phase function can be written as an analytic expression that can be easily altered to fit the physical characteristics of different kinds of cylindrical particles. Furthermore, the reason for interest in a simple and quick model for describing scattering is to integrate the impact of scattering into a model with a larger scope. For example, a two-stream radiative transfer model with multiple atmospheric layers generally uses a phase function to describe the scattering in each atmospheric layer and the results of the radiative transfer model are not significantly altered if such an approximate, instead of exact, phase function is used. Specific types of particles were considered when the phase functions were developed for this report. The motivation for this work was the need for simple phase functions for long fibrous particles and disc-like particles. Numerical phase functions can be cumbersome to generate and do not allow one the physical intuition that might be obtained from examining an analytic form for such a phase function. To this end, the Henyey-Greenstein (H-G) phase function (Henyey and Greenstein, 1941) has been used extensively to describe scattering problems (van de Hulst, 1981). The next section discusses the origin of the H-G phase function and why it is such a natural form for the analytic expression for a phase function. A variation on the H-G phase function with three parameters has been chosen to describe the scattering pattern displayed by cylindrical particles. This phase function should allow sufficient generality to describe the scattering produced by any kind of cylindrical particle (any size or material), provided that some data is available to compare with to determine the three parameters. Later sections of this report discuss numerical phase functions and the comparison of the three-parameter H-G phase function to the numerical phase functions.

2. THEORY AND ORIGIN OF THE HENYEY-GREENSTEIN PHASE FUNCTION

The H-G phase function comes about naturally due to the assumption of spherical symmetry and the use of Legendre polynomials as the polynomials of expansion; and it has gained wide use in scattering descriptions of diverse applications in physics, astrophysics, and meteorology. The H-G phase function is written as

$$p(\theta) = \frac{1 - g^2}{(1 - 2g\cos\theta + g^2)^{3/2}}, \tag{1}$$

where

$$-1 < g < 1, \tag{2}$$

where g is an asymmetry parameter and θ is the scattering angle. The value of g being -1 indicates complete backward scattering, 1 indicates complete forward scattering, and 0 is a uniform or isotropic phase function. Complete forward (or backward) scattering means that the scattering intensity pattern is a delta function in the forward (backward) direction. To derive the H-G phase function, first write the definition of the phase function as an expansion of Legendre polynomials,

$$p(\theta) = \sum_{n=0}^{\infty} w_n P_n(cos\theta). \tag{3}$$

w_n can be written as an expansion of the asymmetry parameter g,

$$w_n = (2n+1)g^n. \tag{4}$$

Now the phase function can be written as

$$p(\theta) = \sum_{n=0}^{\infty} (2n+1) g^n P_n(cos\theta). \tag{5}$$

The phase function can now be written as the sum of two terms, and from that expression the H-G phase function may be obtained as follows:

$$p(\theta) = 2g \sum_{n=0}^{\infty} n P_n(cos\theta) g^{n-1} + \sum_{n=0}^{\infty} g^n P_n(cos\theta). \tag{6}$$

The generating function for the Legendre polynomials is

$$G(x,t) = (1 - 2xt + t^2)^{-1/2} = \sum_{n=0}^{\infty} P_n(x) t^n, \tag{7}$$

where $x = cos\theta$ and $t = g$. The derivative of the generating function is

$$\frac{\partial G}{\partial t} = \frac{x - t}{(1 - 2xt + t^2)^{3/2}} = \sum_{n=0}^{\infty} n P_n(x) t^{n-1}. \tag{8}$$

Recognize the right sides of the above two equations as the two terms in equation (6). These two terms from equations (7) and (8) are substituted into equation (6) and the result is reduced to its simplest form,

$$p(\theta) = \frac{2g(cos\theta - g)}{(1 - 2gcos\theta + g^2)^{3/2}} + \frac{1}{(1 - 2gcos\theta + g^2)^{1/2}} = \frac{1 - g^2}{(1 - 2gcos\theta + g^2)^{3/2}}, \tag{9}$$

which is the H-G phase function.

A more general form for the H-G phase function may be obtained through the use of the generating function of the Gegenbauer or ultraspherical polynomials (Reynolds and McCormick, 1980).

$$P(\theta) = K(1 + g^2 - 2gcos\theta)^{-(\alpha+1)}, \tag{10}$$

where

$$K = \pi^{-1}\alpha g(1-g^2)^{2\alpha}\left[(1+g)^{2\alpha}-(1-g)^{2\alpha}\right]^{-1}\ ,\ \alpha > \frac{-1}{2}, \tag{11}$$

and

$$p(\theta) = 4\pi P(\theta), \tag{12}$$

and $\alpha = 1/2$ gives the H-G function.

There is no practical advantage for using this form of the H-G phase functions in this particular application; in fact, an additional parameter must be specified. Further research into the use of this form of the phase function might prove useful for other ideas.

The H-G phase function is the most widely used analytic form for a phase function (van de Hulst, 1981; Kattawar, 1975), although other forms exist (Reynolds and McCormick, 1980) such as the elliptical or binomial phase functions. The original reference for use of this phase function is for astrophysical work (Henyey and Greenstein, 1941), and the term phase function has its roots in astrophysical lore (van de Hulst, 1981). Since around 1940, the H-G phase function has come into wide usage in meteorology and in scattering research in physics (van de Hulst, 1981).

3. PHASE FUNCTIONS FOR CYLINDRICAL PARTICLES

Four phase functions for cylindrical particles are of particular interest to this work: the numerical phase function resulting from the Extended Boundary Condition Method (EBCM), the form of the phase function resulting from the diffraction limit of the infinite cylinder problem, the numerical phase function for cylindrical particles resulting from Mie theory calculations, and the Rayleigh-Gans phase function for small disc-shaped particles. A quick survey of the available literature revealed that these phase functions were the ones available for cylindrical or disc-like particles. The EBCM models are numerical solutions to electromagnetic equations with specific boundary conditions. The Mie theory calculations are exact solutions. The infinite cylinder and the Rayleigh-Gans method are approximations. Note that the phase function developed in this report is approximate and is compared to the more exact solutions to provide assurance that the approximate form looks somewhat like the exact form.

3.1 Extended Boundary Condition Method

The first of the phase functions discussed is the one resulting from the EBCM. This phase function is numerical but can provide valuable comparison for the three-parameter H-G phase function that has been chosen for the cylindrical particle. The EBCM was developed by Peter Barber (Barber and Yeh, 1975) and is described briefly as follows. A system of

linear equations is obtained for the expansion coefficients of the scattered field in terms of the incident field coefficients. The equations are solved numerically and appear to be most applicable to objects whose physical size is on the order of the wavelength of the incident radiation. The EBCM is a fairly general method and, in fact, can be used to study the index of refraction of the scattering object. In a 1975 paper, Barber and Yeh display plots of phase functions for cylinders, oblate spheroids, and prolate spheroids. The two cases of interest here are the scattering curves for the azimuthal and equatorial planes. All of the curves have the same qualitative shape; that is, maximum intensity in the forward direction, decrease in intensity in intermediate angles (with some oscillation), and a smaller peak in intensity for the backward scattering direction (180 degrees). The data from these plots were digitized and used for comparison to the three-parameter H-G phase function. One useful aspect of this numerical phase function is that Barber and Yeh (1975) have produced numerical phase functions for both prolate and oblate spheroids, which can effectively approximate long thin cylinders and discs in their limiting cases. Barber and Yeh also compare phase functions produced for similarly shaped bodies, prolate spheroids and cylinders.

Figures 1 through 10 are reproductions of the digitized data in Barber and Yeh's 1975 paper. Each of these plots is labeled as in Barber and Yeh , and the figure captions make the plots self-explanatory. The appropriate figures are compared to cylinders and discs in a later section of this report. In these figures several parameters are referred to. These are r, the radius of the sphere; b and a, the axes of the cylindrical particles; and ka, the wavenumber times the radius of the particle. This quantity is later referred to as the size parameter. The dielectric constant, ϵ_r, or the optical constants are also given in the figure descriptions. The vertical polarization referred to in the figures is perpendicular to the scattering plane, and the horizontal polarization is parallel to the scattering plane. Although some of these figures did not result in phase functions that were used in the comparisons in this report, all of the Barber and Yeh phase functions that were digitized are included here to give a feeling for the scope of the Barber and Yeh work. The ultimate use of the phase functions developed by Barber and Yeh (1975) is most probably different from the one envisioned here in this report. The author of this report felt that the Barber and Yeh phase functions were probably quite accurate, but computationally intensive. The EBCM phase functions shown here are just digitized from specific examples given in papers by Barber and Yeh.

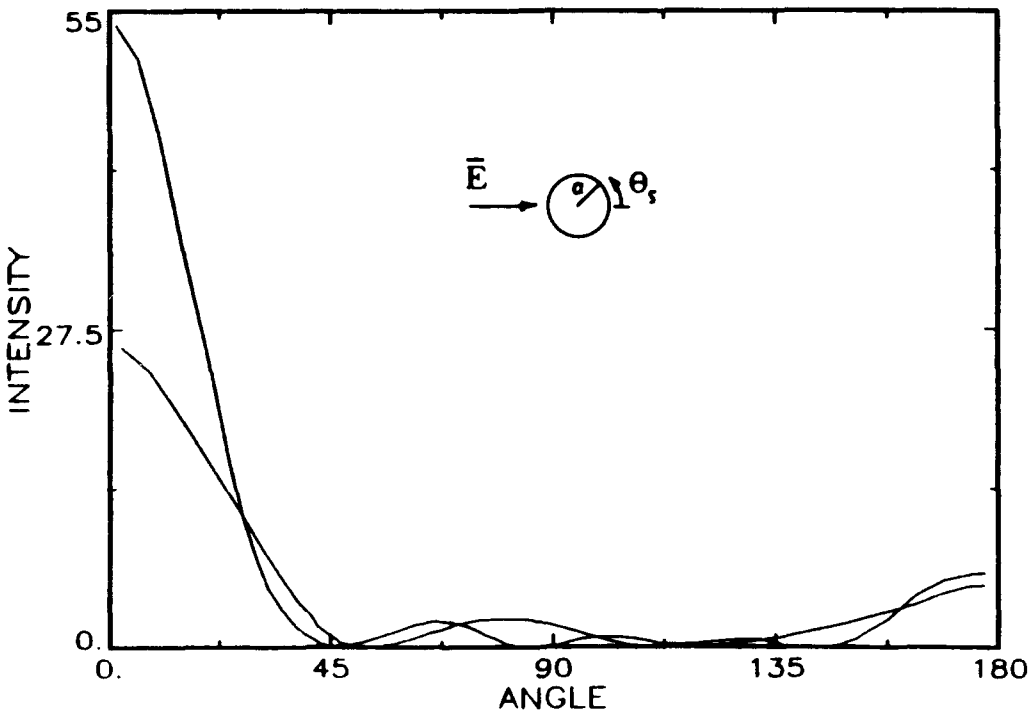

Figure 1. Barber-Yeh figure 9 sphere scattering, vertical polarization, ka=3.0,5.0, dielectric constant $\epsilon_r = 4.0$.

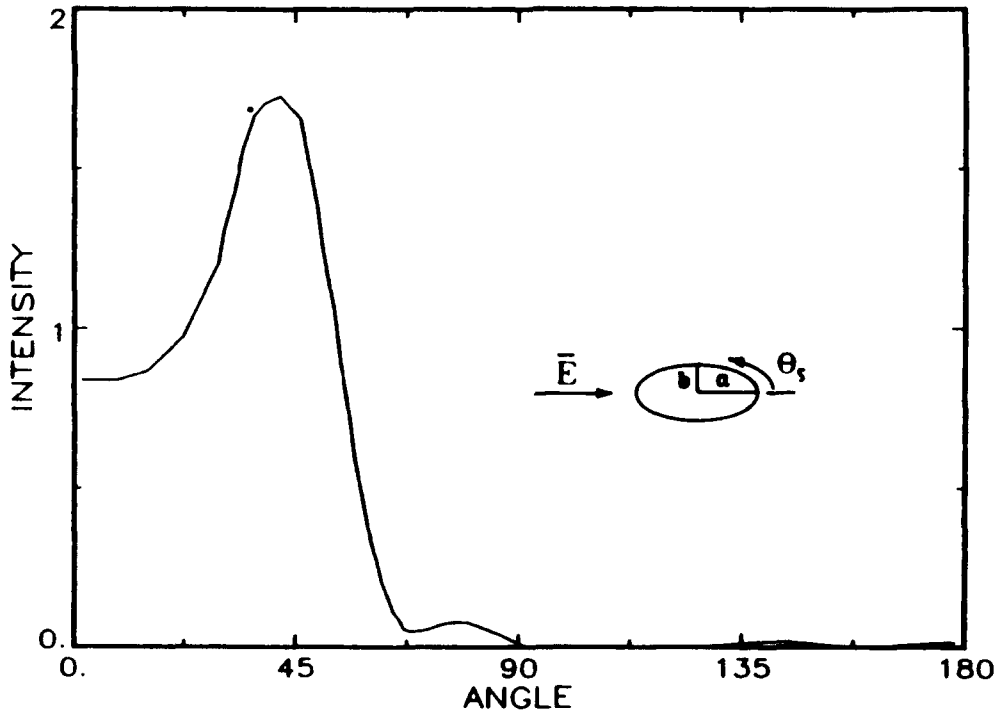

Figure 2. Barber-Yeh figure 10a prolate spheroid scattering, vertical polarization, ka=7.114, $\epsilon_r = 5.0$, $\frac{b}{a} = \frac{1}{3}$, azimuthal plane.

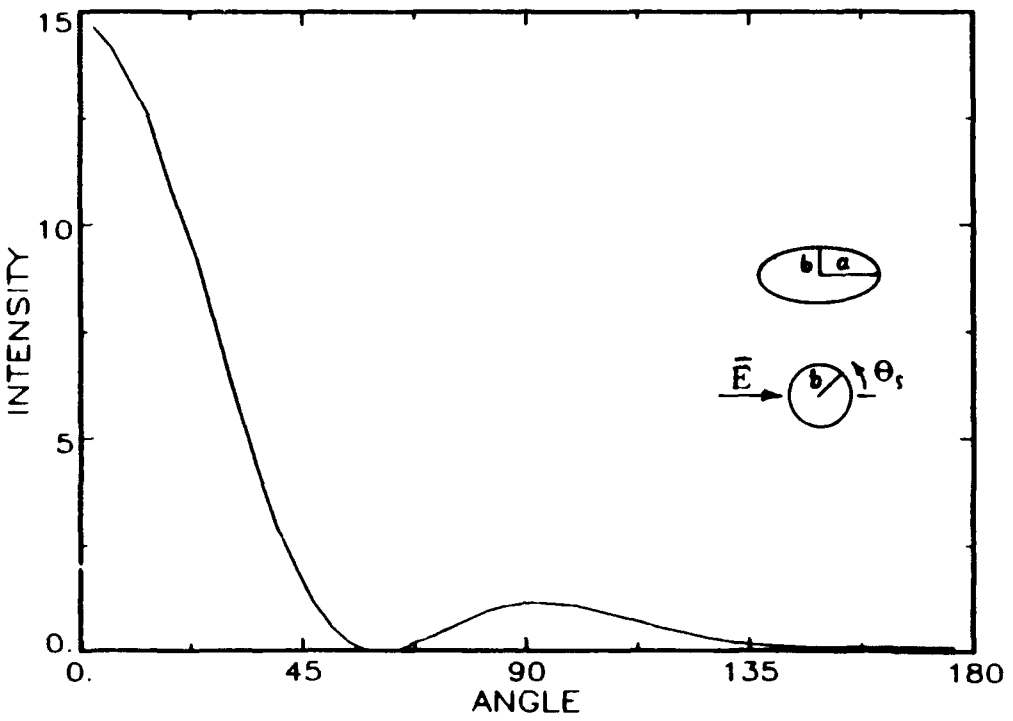

Figure 3. Barber-Yeh figure 10b prolate spheroid scattering, vertical polarization, ka=7.114, $\epsilon_r = 5.0$, $\frac{b}{a} = \frac{1}{3}$, equatorial plane.

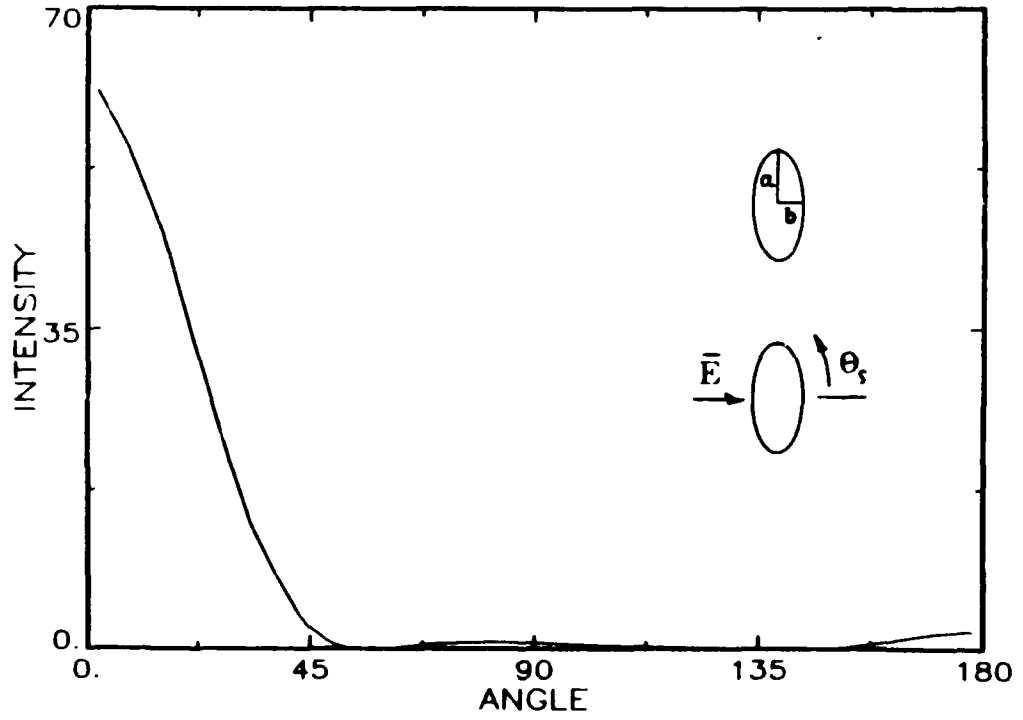

Figure 4. Barber-Yeh figure 11a oblate spheroid scattering, vertical polarization, ka=4.932, $\epsilon_r = 5.0$, $\frac{b}{a} = \frac{1}{3}$, azimuthal plane.

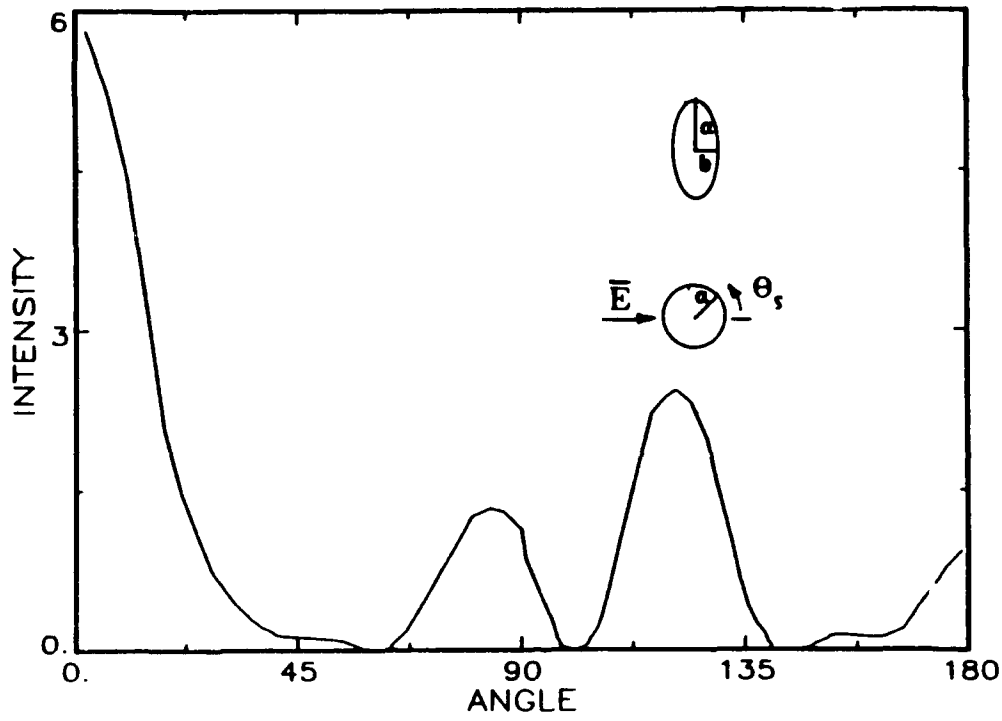

Figure 5. Barber-Yeh figure 11b oblate spheroid scattering, vertical polarization, ka=4.932, $\epsilon_r = 5.0$, $\frac{b}{a} = \frac{1}{3}$, equatorial plane.

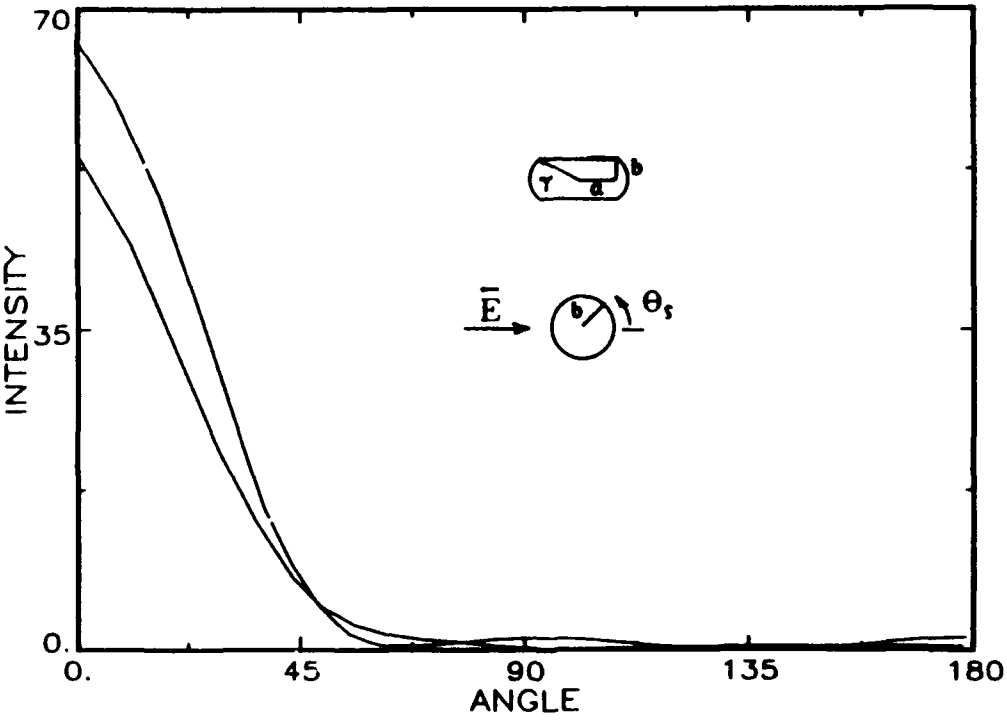

Figure 6. Barber-Yeh figure 12a cylinder scattering, equatorial plane, ka=5.288, $\epsilon_r = 1.96$, $\frac{b}{a}$=0.577, $r = 2b$, both vertical and horizontal polarization shown, vertical has more minima.

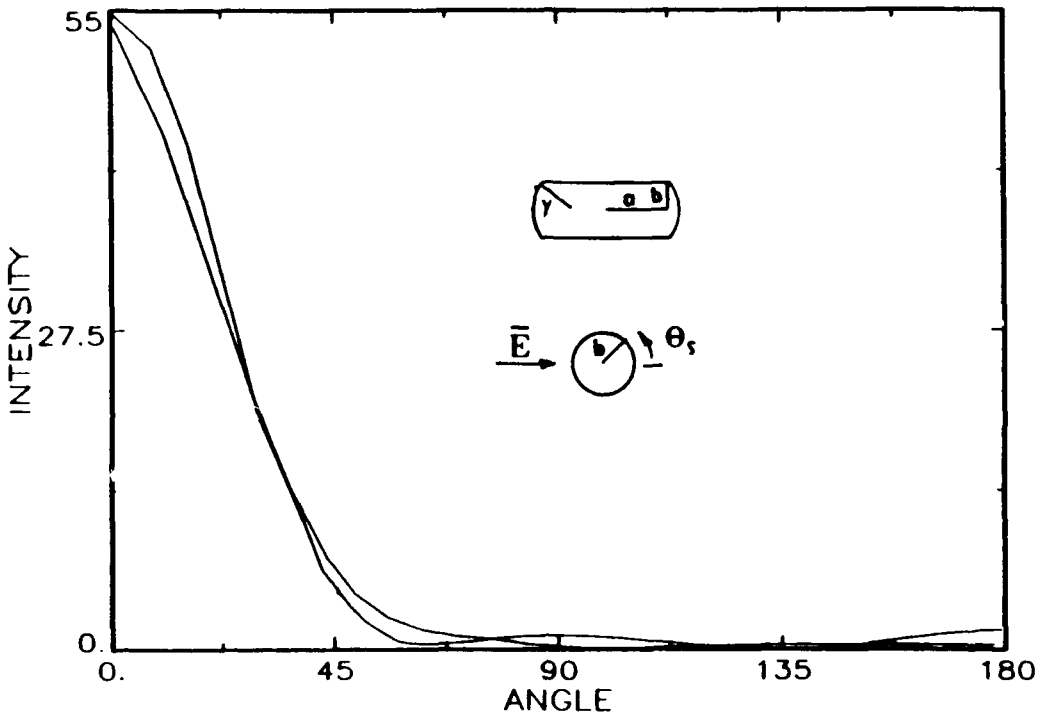

Figure 7. Barber-Yeh figure 12b cylinder scattering, equatorial plane, $r = 2b$, ka=8.341, $\epsilon_r = 1.96$, $\frac{b}{a}$=0.366, both vertical and horizontal polarizations shown, vertical has more minima.

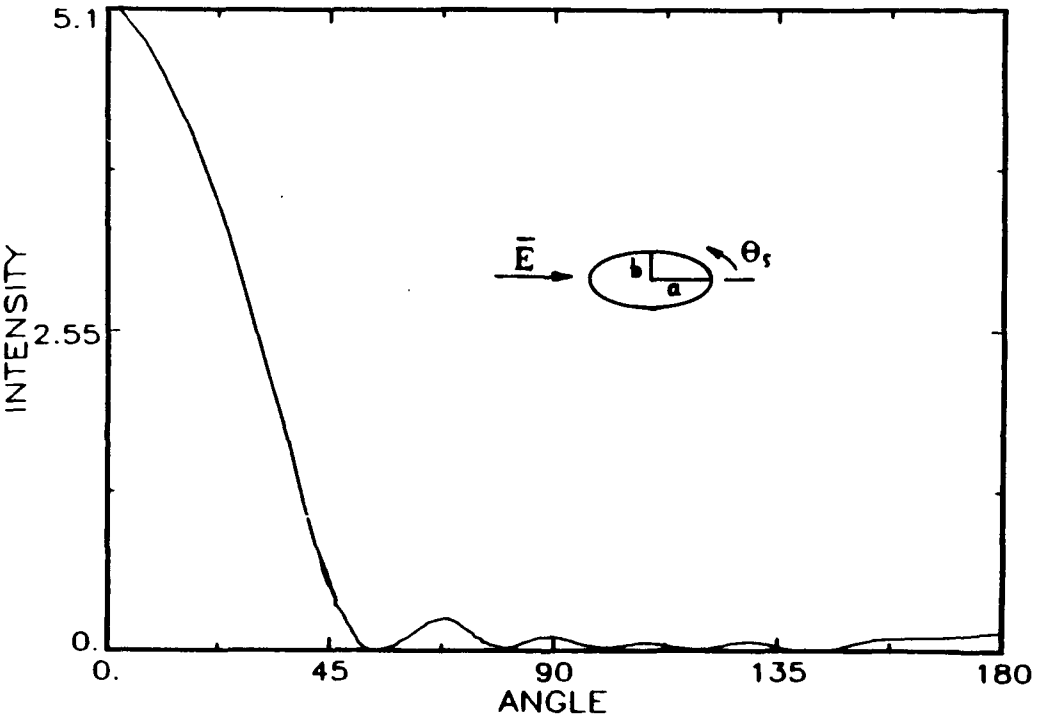

Figure 8. Barber-Yeh figure 13a scattering by a prolate spheriod, vertical polarization, azimuthal plane, $\epsilon_r = 2.28$, ka=9.529, $\frac{a}{b}$=2.0, prolate spheroid.

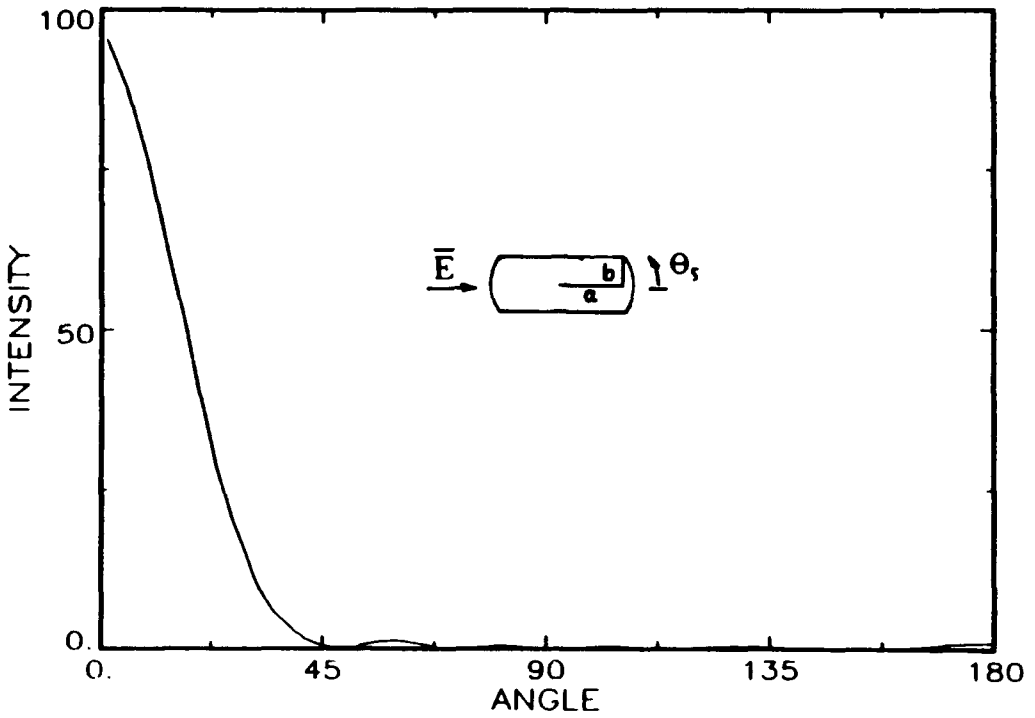

Figure 9. Barber-Yeh figure 13b scattering by a capped cylinder having the same length and width as the prolate spheriod in figure 2.8, vertical polarization, azimuthal plane, ka=4.765, ϵ_r = 2.28, $\frac{a}{b}$=1.0, cylinder.

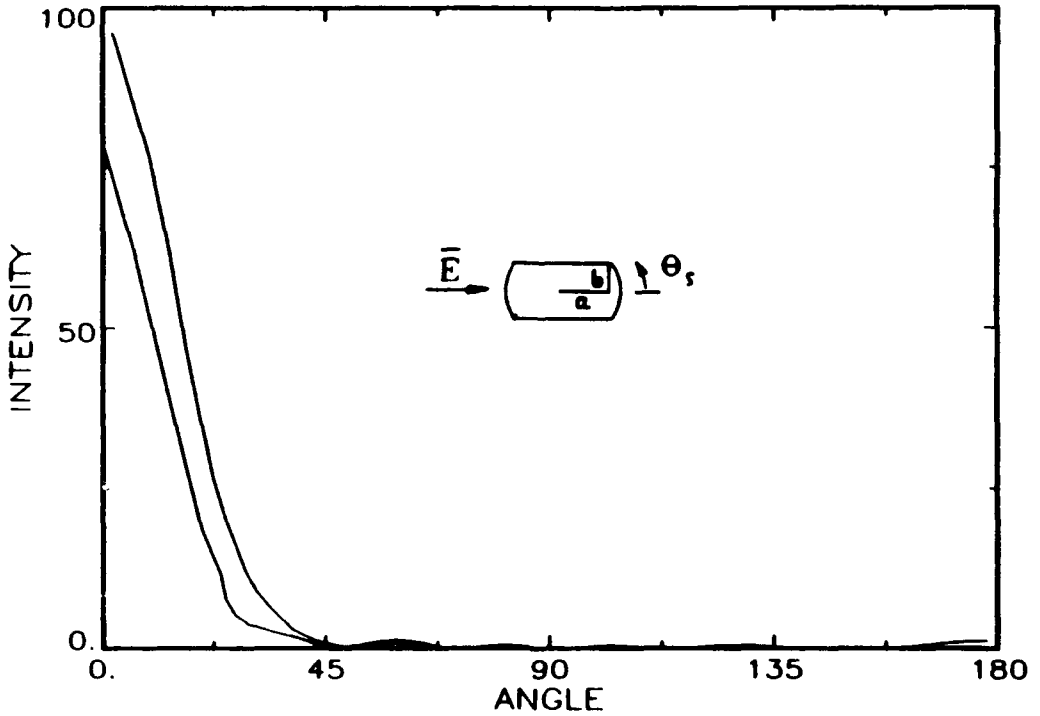

Figure 10. Barber-Yeh figure 14 cylinder scattering, azimuthal plane, vertical polarization, ka=4.765, $\frac{a}{b}$=1.0, m=1.51, m=1.51-j0.05.

The prolate spheroids are compared to the long thin cylinders, and the oblate spheroids may be compared to disc-like particles. Note here that in the original paper (Barber and Yeh, 1975), these plots were expressed with the y-axis as a logarithmic scale, so the plots in this report may appear somewhat different because of the change in scale. The logarithmic scale is not used for these plots because the other phase functions are not expressed logarithmically, and for comparison purposes, the scales should be the same. Another feature to note is that the incidence of the radiation that is scattered is denoted on the plots, as it is on the original plots. For comparison purposes using the EBCM phase function, figure 7 is the closest to the case of the essentially infinite cylinder (where the length is 10 times the size of the diameter) that is simulated by the EBCM model.

Additionally, Mott and Brown (1984) studied the EBCM as applied to small spheres and oblate spheroids. They caution that although the EBCM may be applied to nonspherical, rotationally symmetric particles, care must be taken in the interpretation of the results of this method. The numerical computer code has convergence problems under certain conditions, and therefore, when using limiting cases of spheroids to describe cylinders, care must be taken to see that convergence problems do not affect the results.

3.2 Diffraction-Limited Phase Function

Bohren and Huffman (1983) extensively discuss scattering by an infinite right circular cylinder. After the scattering problem is discussed in general, several special cases are discussed in particular. One of these special cases discussed is the diffraction theory limit. According to diffraction theory, an opaque cylinder, an opaque rectangular obstacle, and a rectangular aperture in an opaque screen, all with the same projected cross sectional area, scatter light in the same manner independently of the polarization of the incident light. Bohren and Huffman's development provides the reader with an objective criterion with which to judge the limits of diffraction theory. This criterion says that when the ratio of the length (L) of the cylinder and the diameter ($2a$) exceeds 10,

$$R = \frac{L}{2a} > 10, \tag{13}$$

the cylinder may be considered essentially infinite. When $R > 10$, there is little light scattered in directions other than those in a plane perpendicular to the cylinder axis. The larger R is in value, the more scattered light is concentrated in this direction. For a truly infinite cylinder, the scattered light exists only in this plane perpendicular to the cylinder axis. Using this concept in their analysis, Bohren and Huffman (1983) obtain a closed form expression for the phase function for infinite cylinders in the diffraction theory limit

$$p(\theta) = \frac{\pi}{4x}\left[\frac{1+cos\theta}{\pi}\frac{xsin(xsin\theta)}{xsin\theta}\right]^2, \tag{14}$$

where $x = ka$ and which is normalized,

$$\int_{-\pi}^{+\pi} p(\theta) d\theta = 1 \tag{15}$$

This form for the phase function vanishes in the backward direction and at angles where $sin\theta = n\pi/x$, where n is an integer. Diffraction theory is a good approximation when the diameter of the cylinders is large. It provides a means of estimating the diameter (d) as the wavelength (λ) times the number of minima (n_{min}) in the phase function between 0 and 90 degrees,

$$d \cong \lambda n_{min}. \tag{16}$$

Diffraction theory is at its best for large opaque cylinders where opaque is meant in the sense of nonreflecting and totally absorbing. Figure 11 is shown here as representative of a phase function produced by this diffraction limited theory. Note that the larger the value of $x = ka$, the more sharply peaked the forward scattering.

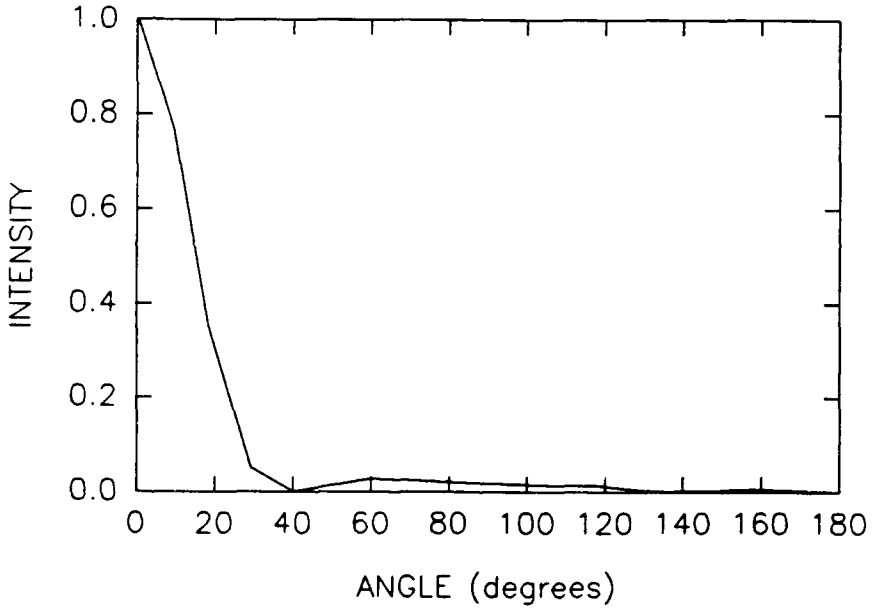

Figure 11. Cylinder scattering, diffraction limit, infinite cylinder, $x = ka$ =5.0.

The point made here in diffraction theory, that there is essentially no scattering intensity except in the plane normal to the cylindrical axis, for infinite cylinders is very important to this analysis. Since fiber-like cylindrical particles will almost always be considered infinite by the criterion mentioned above, the azimuthal dependence of the scattering can be ignored and it may be assumed that the scattering is almost all in the plane normal to the axis of the cylinder.

All phase functions produced for this report, except those that were digitized from the Barber and Yeh (1975) paper, are normalized to 1. This means that the area under the different

phase function curves may not be equal, but an attempt is made only to reproduce the general shape of the phase function for cylinders with this simple analytic form.

3.3 Cylindrical-Mie Theory (Exact Solution)

This method is referred to as Cylindrical-Mie (C-M) theory when in the strict sense Mie theory refers to scattering by spheres, and this is a discussion on scattering by cylinders. This section is called C-M theory because the solution for the infinitely long cylinder is obtained by the same method of solution as in the case for spheres. Bohren and Huffman (1983) thoroughly discuss the solution for the scattering coefficients in terms of Bessel and Hankel functions in chapter 8 and appendix C of their book. Therefore, the reader is referred to this reference for the details of this calculation.

Bohren and Timbrell have written a C-M program to compute the phase function (among other things) for an infinitely long cylinder. This program is listed in an appendix of Bohren and Huffman's (1983) book.

This C-M program is used for comparison with the assumption that for all practical purposes infinite cylinders are always used, since the ratio of the length to the diameter of the particles considered here is greater than 10. The C-M program has been modified to allow several items as input in this program. These items are the refractive index of the surrounding medium, the real and imaginary refractive indices of the cylindrical particle, the particle radius, the wavelength of the incident light, and the scattering angle being printed out in degrees or radians. This modification of the program allowed us to determine the sensitivity of the calculation to various parameters such as the pertinent refractive indices. This is discussed more fully in the next section; however, here figure 12 shows a representative plot of a phase function produced by this program. This is the phase function produced for a graphite fiber with real and imaginary refractive indices of 1.8 and 1.6. The cylinder radius is 12.5 μm, and the incident radiation wavelength is .53 μm. This gives a size parameter of 148.2. Table 1 lists the C-M program output for this case. For this particular case the last column, labeled t34, contains values that are identically zero and they have been omitted in table 1.

3.4 Rayleigh-Gans Theory

It is possible to obtain relatively simple approximate expressions for the scattering matrix elements when the particles are small, but not so small as in the limit of Rayleigh scattering, and when they are suspended in a medium with similar optical properties. This latter characteristic is sometimes referred to as "soft" or "tenuous." In quantum mechanical scattering this is referred to as the first Born approximation. Others have also contributed to

this area of scattering theory (Bohren and Huffman, 1983; Ishimaru, 1977). A closed form approximate solution may be obtained for the finite cylinder under these circumstances, and it is best applied to discs. The phase function is the square of the form factor given here as

$$f(\theta, \phi, \gamma) = \frac{2sin(x\mathcal{L}A)}{x\mathcal{L}A} \frac{J_1(xM)}{xM}, \tag{17}$$

where γ is the angle of incidence, $\mathcal{L}$ is L/a, $x = ka$, $A = cos\gamma + sin\theta cos\phi$, $B = sin\theta sin\phi$, $C = cos\theta - sin\gamma$, $M = \sqrt{B^2 + C^2}$, and the cylinder and the various angles are depicted in figure 13. Figure 14 is a plot of the phase function produced by using a special case of equation (16) described in equation (17). This approximate form of the phase function is probably best applied to a disc and is really only applicable to the regime of smaller particles than those in which there is an interest here.

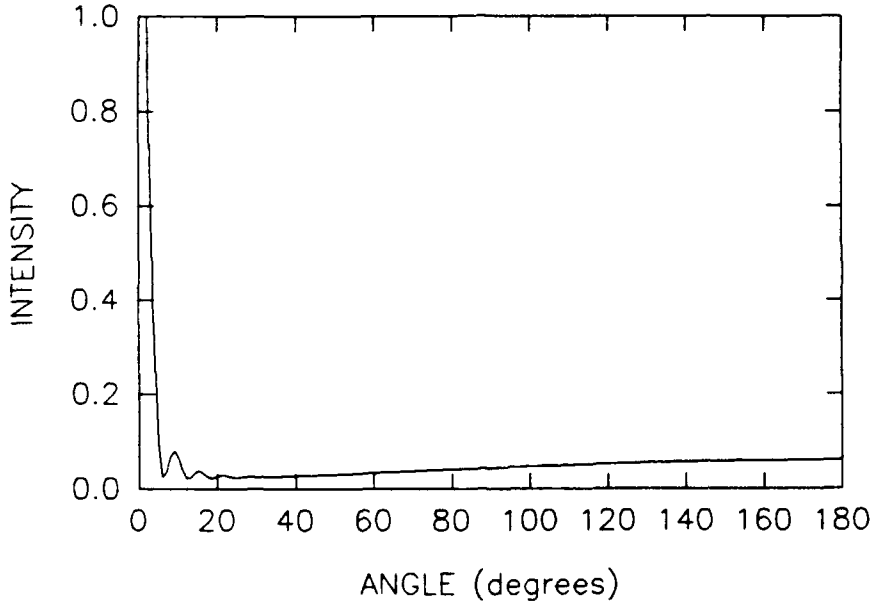

Figure 12. Cylinder scattering, Bohren-Mie type calculation for graphite indices, 1.8, 1.6; wavelength = 0.53 μm, cylinder radius 12.5 μm.

Table 1. Cylinder Program : Normally Incident Light

```
refmed = 1.0000, refre = 0.180000E+01, refim =
0.160000E+01
cylinder radius = 12.500, wavelength = 0.5300
size parameter = 148.1888
Other output :
qscpar = 0.378438E-02, qexpar = 0.380554E-02
qscper = 0.379179E-02, qexper = 0.380489E-02
```

radians	t11	pol	t33
0.00	0.100000E+01	-0.978495E-03	0.100000E+01
0.16	0.983652E+00	-0.962302E-03	0.100000E+01
0.31	0.935807E+00	-0.912258E-03	0.100000E+01
0.47	0.859955E+00	-0.824511E-03	0.100000E+01
0.63	0.761567E+00	-0.691964E-03	0.100000E+01
0.79	0.647603E+00	-0.501718E-03	0.100000E+01
0.94	0.525901E+00	-0.233838E-03	0.100000E+01
1.10	0.404489E+00	+0.146042E-03	0.100000E+01
1.26	0.290893E+00	+0.699678E-03	0.100000E+01
1.41	0.191515E+00	+0.154635E-02	0.999999E+00
1.57	0.111112E+00	+0.295097E-02	0.999995E+00
1.73	0.524619E-01	+0.563468E-02	0.999982E+00
1.88	0.162119E-01	+0.124874E-01	0.999911E+00
2.04	0.941919E-03	+0.610435E-01	0.997873E+00
2.20	0.342614E-02	-0.365026E-01	0.999240E+00
2.36	0.190648E-01	-0.171720E-01	0.999832E+00
2.51	0.424419E-01	-0.124800E-01	0.999911E+00
2.67	0.679506E-01	-0.104803E-01	0.999937E+00
2.83	0.904244E-01	-0.947692E-02	0.999949E+00
2.98	0.105708E+00	-0.898619E-02	0.999954E+00
3.14	0.111112E+00	-0.883741E-02	0.999955E+00

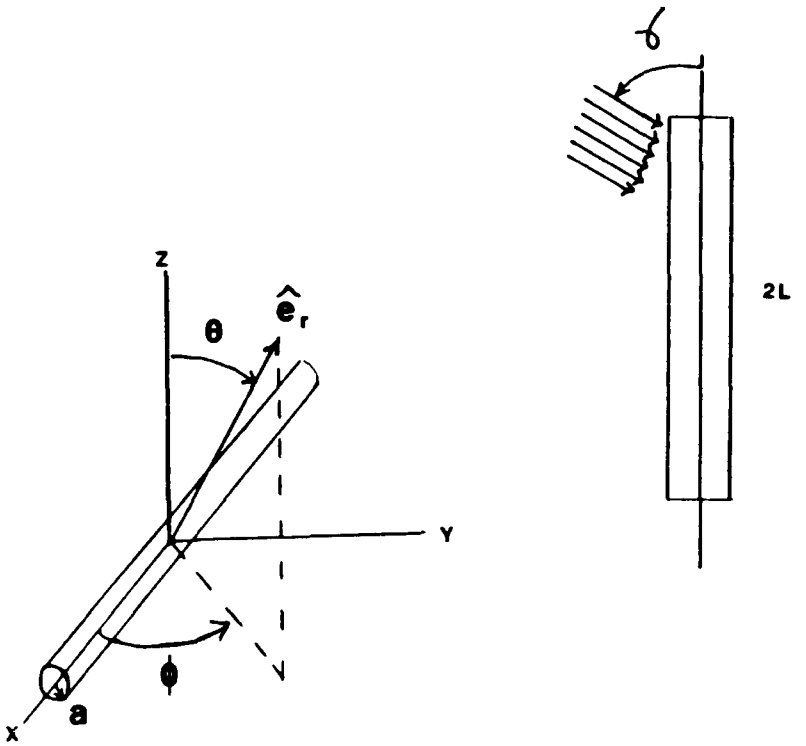

Figure 13. A finite cylinder illuminated obliquely.

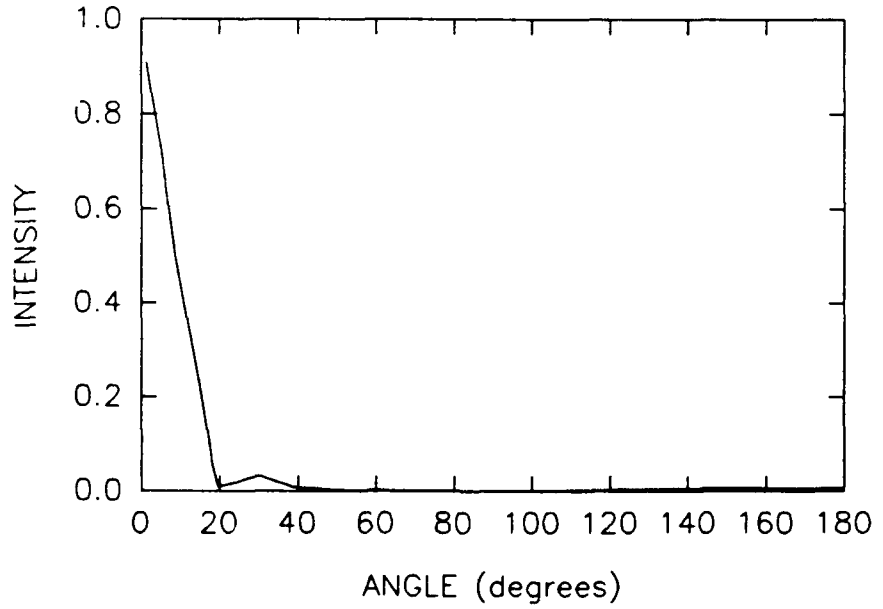

Figure 14. Rayleigh-Gans approximation, normalization=3.99, cylinders in disk-like limit.

In the case of the light being normally incident to the cylindrical axis, that is, when $\gamma = \pi/2$ is a plane normal to the axis ($\phi = \pi/2$ or $3\pi/2$), equation (16) reduces to

$$f(\theta) = \frac{2J_1\left(2x\sin\frac{\theta}{2}\right)}{2x\sin\frac{\theta}{2}} \tag{18}$$

All of the phase functions discussed in this report except for those generated by EBCM theory and the C-M theory were calculated from the equations shown in the text.

4. COMPARISON OF DOUBLE H-G PHASE FUNCTION TO OTHER PHASE FUNCTIONS

Three analytic forms are considered here for a phase function for cylindrical particles in this report. Two of these forms are for specific cases and do not appear to be general enough or fit the numerical phase functions well enough to be used as phase functions for cylinders. The third analytic phase function arose from ideas about how a phase function for a cylinder might relate to that of a sphere and from the work of others (Kattawar, 1975; Reynolds and McCormick, 1980). The two less useful phase functions are discussed first below, and then the new analytic phase function for a cylinder is introduced and discussed in comparison to the numerical phase functions for cylinders.

First the case for the disc-like particles is discussed. For this case, the Rayleigh-Gans theory phase function is compared to the oblate spheroid phase function digitized from the EBCM paper (Barber and Yeh, 1975). The oblate spheroid phase functions in this report are figures 4 and 5. Figure 4 is in the azimuthal plane, and figure 5 is in the equatorial plane. Figure 15 is a comparison of the phase function produced by using the Rayleigh-Gans theory and the phase function produced by the oblate spheroid in the EBCM theory. In both cases the value of $x = ka$ is approximately the same, $x = 5.0$. The correlation between the two phase functions appears to be good; however, one must remember that this form of the phase function is good only for small particles and in this specific case, for discs. These constraints severely limit the applicability of this form of the phase function. For this reason, this form of the phase function is not chosen for the general analytic form of the phase function.

Next, compare the phase function produced by the diffraction limit theory to the EBCM cylinder phase function and the C-M phase function. First, the comparison is made between the diffraction-limit phase function and the EBCM method in figures 11 and 7. This is shown in figure 16. Figure 17 is the same comparison, but the value of ka has been changed in the diffraction-limited model to more closely match the value of ka in the EBCM model. A closer match to the EBCM model phase function (figure 18) is produced by lowering the value of ka to approximately 2.8. The reader is cautioned that all of the phase functions used here are normalized to 1, but in figure 18, the areas under the phase function curves

are nearly the same. In figure 18 the size parameters of the two phase functions differ by about a factor of 3, but the curves match fairly closely. These figures illustrate that there is some disagreement even among well-accepted models.

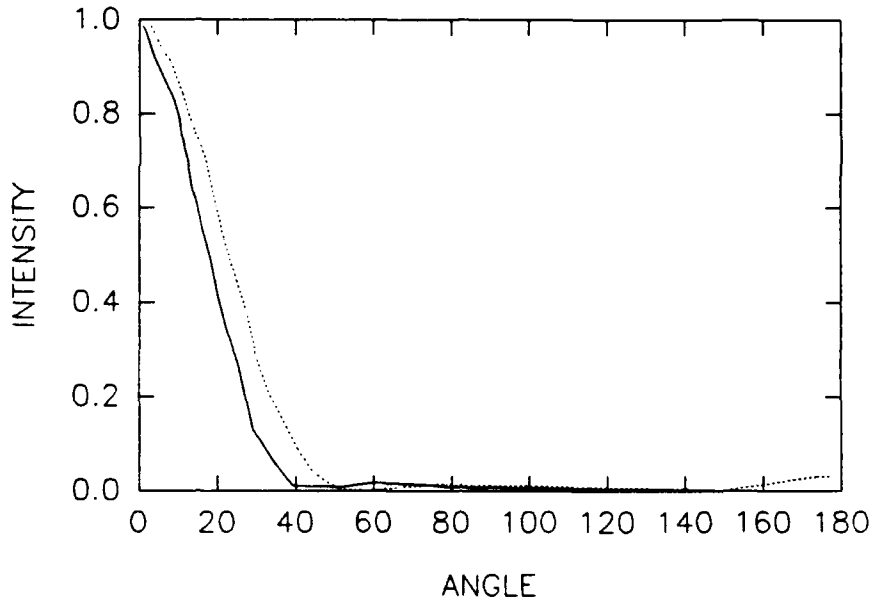

Figure 15. Rayleigh-Gans approximation, normalization=0.99 (solid line), EBCM oblate spheroid. ka=4.932 (dashed line).

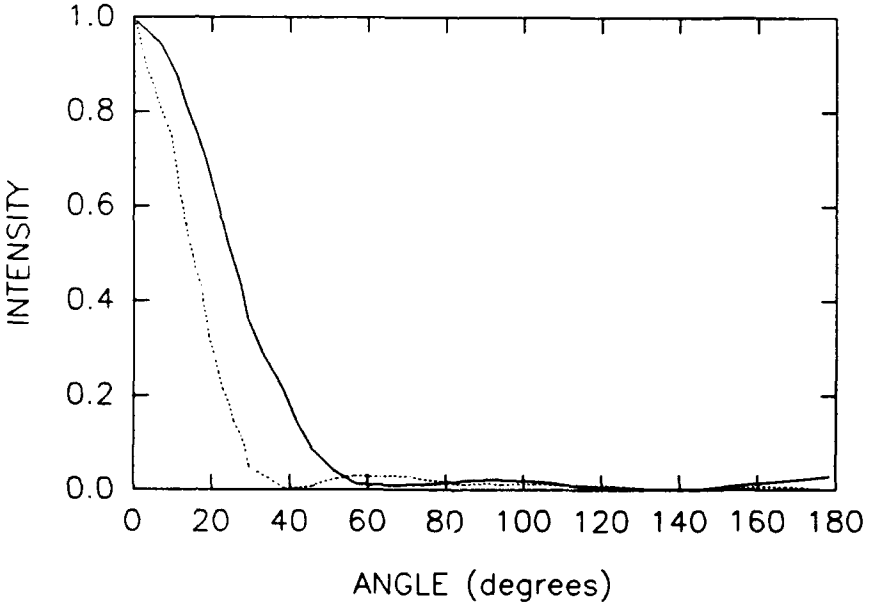

Figure 16. Cylinder scattering, diffraction limited case, ka=5.0 (dashed line), EBCM cylinder, ka=8.341, $\frac{b}{a}$=0.366 (solid line).

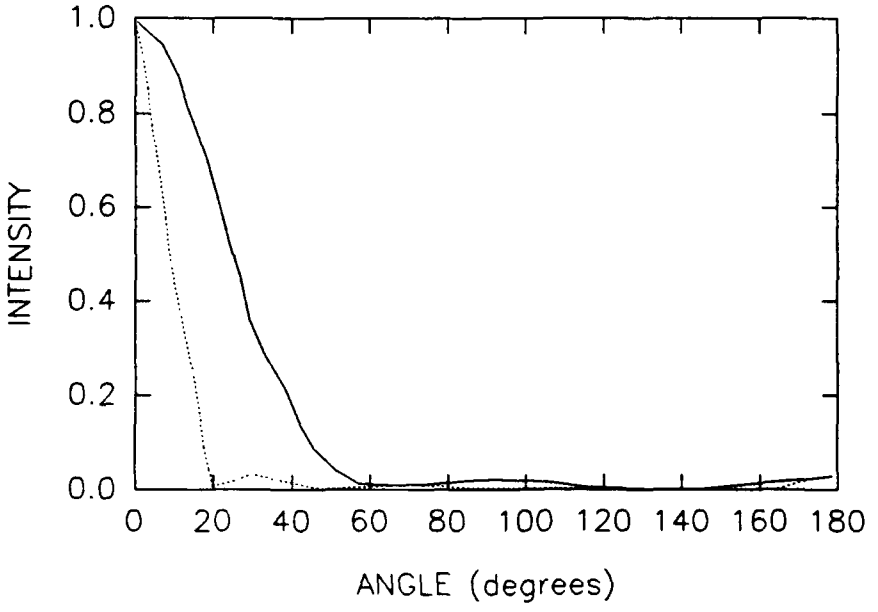

Figure 17. Cylinder scattering, diffraction limited case, ka=8.341 (dashed line); EBCM cylinder, ka=8.341, $\frac{b}{a}$=0.366 (solid line).

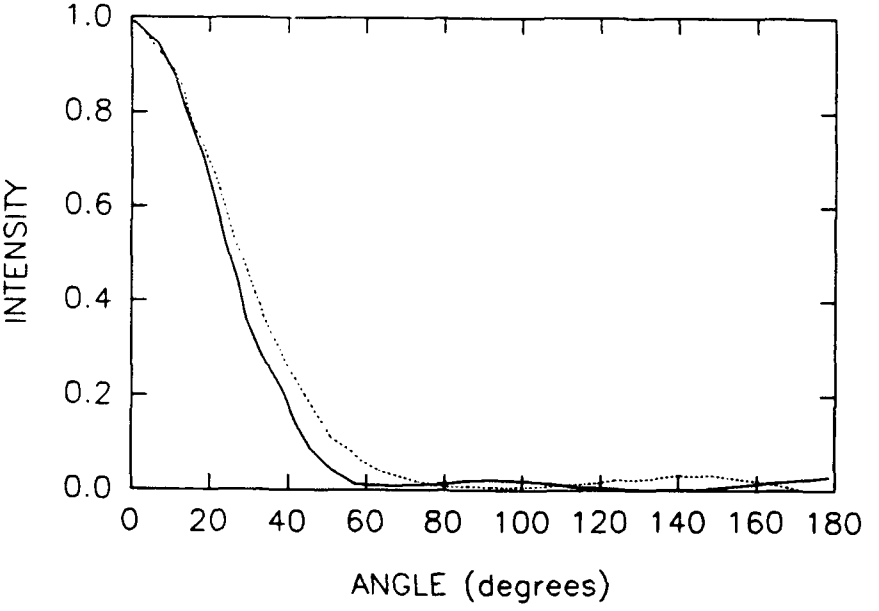

Figure 18. Cylinder scattering, diffraction limited case, ka=2.8 (dashed line); EBCM cylinder, ka=8.341, $\frac{b}{a}$=0.366 (solid line).

Figures 19 and 20 are comparisons between the diffraction-limited phase function and the C-M phase function. The C-M phase function is narrower than the diffraction-limited case, but both show strong forward scattering and a little backward scattering. Some general observations may be made about the comparisons made in figures 16 through 20. Both the diffraction-limited case and the C-M theory assume an infinite cylinder, but the EBCM does not. One may conclude, then, that the assumption of an infinite cylinder does cause the phase function to be more narrowly peaked in the forward direction. Recall also that the infinite cylinder is a good approximation for the finite cylinder if the ratio of the length to diameter is 10 or greater. Using the minimum diameter criterion, equation (15), one can conclude that the size particle considered here certainly more than meets this criterion. The diffraction-limited case is at its best for opaque particles, where opaque means that the particle does not reflect the incident light and absorbs the transmitted light. No real particle meets this criterion; such a particle would have a real refractive index the same as the surrounding medium. This is similar to one of the criteria for the Rayleigh-Gans theory. Similarly, this diffraction-limited theory is approximate; therefore, although this form of the phase function may be useful in certain cases, it will not be used for the general analytic phase function either.

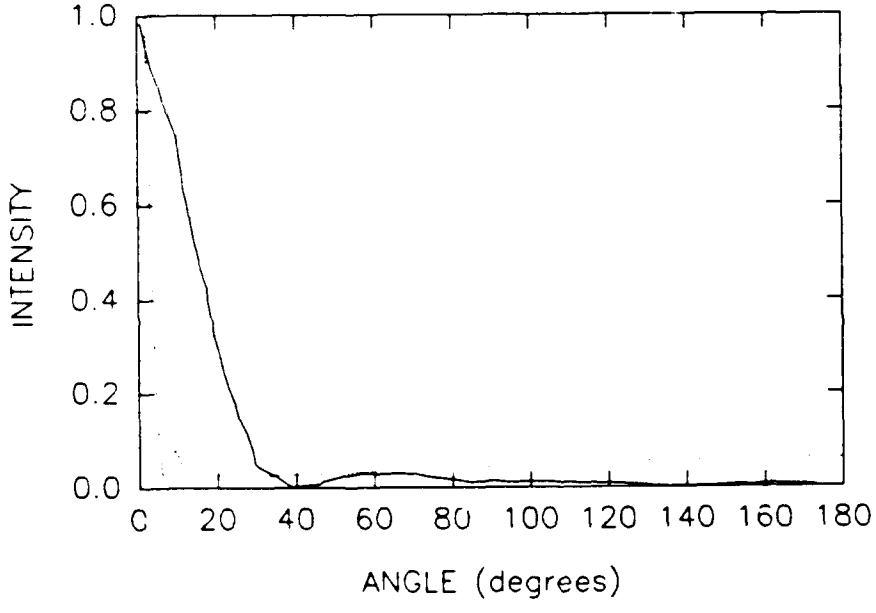

Figure 19. Cylinder scattering, diffraction limited case, ka=5.0 (solid line); C-M theory phase function, graphite (dashed line).

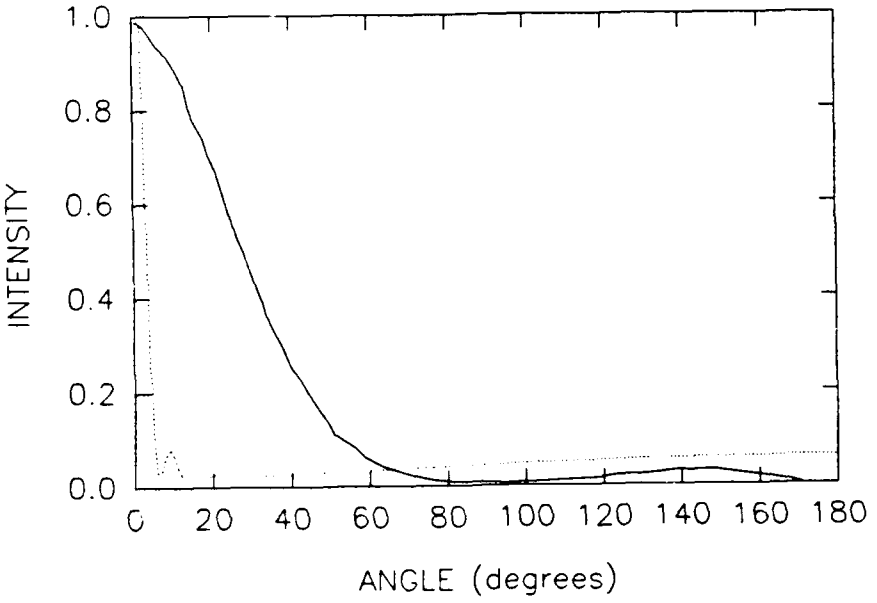

Figure 20. Cylinder scattering, diffraction limited case, ka=2.8 (solid line); C-M theory phase function, graphite (solid line).

A three-parameter phase function has been used to fit to the first three Legendre coefficients (Kattawar, 1975). This same form of the three-parameter phase function is used here, but it is matched instead to the form of the phase function produced by the EBCM theory and the C-M theory.

The three-parameter phase function is the weighted sum of two H-G functions,

$$p(\theta) = \frac{\beta(1-g_1^2)}{(1-2g_1 cos\theta + g_1^2)^{3/2}} + \frac{(1-\beta)(1-g_2^2)}{(1-2g_2 cos\theta + g_2)^{3/2}}, \tag{19}$$

where β is the relative weight between the two H-G phase functions and g_1 and g_2 are the two asymmetry factors for the two different H-G functions. Kattawar takes the three parameters and writes three equations in terms of these parameters from the first three coefficients of the Legendre polynomials in the expression for the phase function,

$$p(\theta) = \frac{1}{4\pi} \sum_{n=0}^{\infty} (\beta g_1^n + (1-\beta) g_2^n)(2n+1) P_n(cos\theta). \tag{20}$$

Each coefficient is assigned a symbolic value, and the three equations are solved in terms of the coefficients for the three parameters. A phase function can be written in terms of a sum of more than two H-G functions. This same method of solution for the parameters can be used, but there will be a larger number of equations to solve. The number of simultaneous equations will depend on the number of H-G functions and their relative weights. The model is limited to the sum of two H-G functions because it appears to adequately model the

behavior of the phase function, without unnecessarily complicating it. The sum of two H-G functions can give a scattering peak both in the forward and backward direction, depending on the values of the asymmetry factors and the relative weight.

Figure 21 shows a variety of three parameter H-G phase functions with the parameters listed in parentheses under the figure. The values in the brackets are the parameters in the order g_1, g_2, and β. The curves are labeled according to the order that the parameters are listed on the right side of the plot. The amount of backscattering and the width of the forward scattering peak can be varied by varying the values of the parameters.

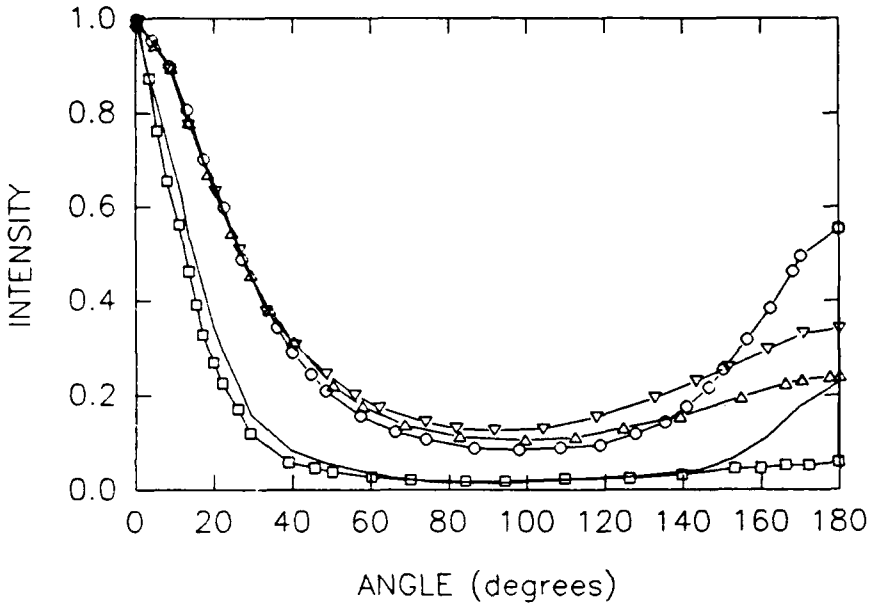

Figure 21. Three-parameter Henyey-Greenstein phase function : solid line (0.71,-0.65,0.75), with circles (0.55,-0.55,0.65), with inverted triangles (0.55,-0.35,0.55), with boxes (0.75,-0.35,0.65), with triangles (0.55,-0.35,0.65), and same as inverted triangles (0.45,-0.35,0.55).

First is the comparison of the double H-G phase function to the C-M phase function. The C-M phase function did not appear to be very sensitive to variation in cylinder radius, refractive index, or wavelength, at least in the visible wavelength range for large cylinders. Graphite was chosen as a material representative of the type of long cylinders or fibers that is modeled here. The refractive indices of graphite are 1.8 (or 2.2) for the real part and 1.6 for the imaginary part (Gillespie and Goedecke, 1989). A visible wavelength of .53 μm, a cylinder radius of 12.5 μm, and a size parameter of 148.2 are chosen. Figure 12 is a plot of the phase function of such a particle computed using C-M theory. The parameters for this particle reflect the characteristics of an obscuration aerosol for military applications. Figure [illegible] a comparison of the phase function for graphite computed by using the C-M theory and

a double H-G function. Phase functions can be plotted as polar plots or rectilinear figures. When plotted as rectilinear figures as shown here, the forward scattering is in the direction of 0° and backward scattering is in the direction of 180°. The relative heights of both the forward and backward scattering peaks match fairly well, although the width of the forward scattering peak is not as good a match as for some phase functions. There is relatively greater scattering intensity at the intermediate angles for the case of the C-M theory than the H-G phase function form considered here. Although this indicates that the C-M theory gives more isotropic scattering than the H-G model, the difference is slight.

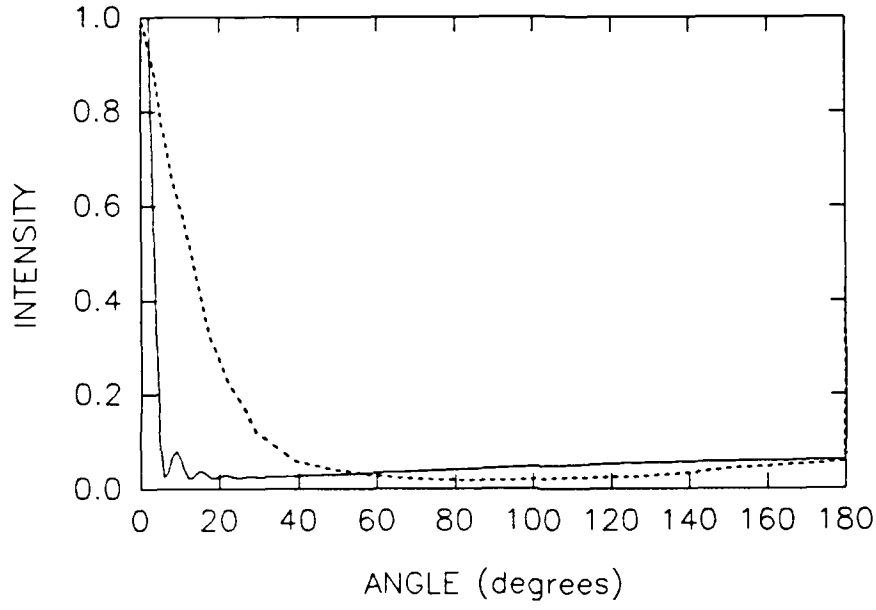

Figure 22. Phase function for cylinders, C-M theory for graphite (1.8,1.6) (solid line): H-G phase function with parameters (0.75,-0.35,0.65) (dashed line).

Investigation of the form of the H-G phase function shows that it is a highly peaked function. Experimentation with a variety of combinations of parameters shows that to get the forward peak and small backward peak to the phase function for the cylinder, one must decrease the value of the second asymmetry factor to a value of about half of the first asymmetry parameter. The relative weight between the two asymmetry values is 0.65. The two asymmetry values are $g_1 = 0.75$ and $g_2 = -0.35$. Any use of the approximate phase function developed in this report should be tempered by a knowledge of the shortcomings and limitations of the model.

Since the forms of the two curves in figure 22 have somewhat similar shapes, it can be said that the parameters $g_1 = 0.75$, $g_2 = -0.35$, and $\beta = 0.65$ provide the best fit of the double H-G function to the C-M phase function curve for graphite. It is recognized that the shapes of the curves may be similar, but the widths of the forward scattering peaks are different. A least squares fit to the functional form of the double H-G function is not possible because two of the least squares equations are identical, and a unique solution is therefore not possible. This is due to the actual functional form of the double H-G phase function.

The double H-G function was also compared to the phase functions produced by the EBCM. The EBCM phase function in figure 7 was chosen to compare to the double H-G phase function because the particle it represents most closely resembles the fibrous particles that are being modeled. The ratio of the length to the diameter of the cylinder in figure 7 is 3, which does not quite meet the requirements for the essentially infinite cylinder mentioned previously in this report. Of all the particles for which phase functions are produced in the EBCM paper (Barber and Yeh, 1975), this particle has the largest length to diameter ratio.

By examining of the figures in the EBCM paper (Barber and Yeh, 1975), one can see that as the length of the cylinder increases, the intensity of the backward scattering component increases. One should remember this as the comparison to the double H-G function is made. Figure 23 is such a comparison. The EBCM phase function in figure 23 is from figure 7 in Barber and Yeh's paper, and the double H-G phase function has parameters $g_1 = .75$, $g_2 = -.35$, and $\beta = .65$. These parameters are the same as those derived by comparison to the C-M theory. It is apparent in this case that the double H-G underestimates the width of the forward scattering, but the forward and backward intensities match. The EBCM theory shows more structure at intermediate angles. The general shape of the phase function is about the same.

By comparison to the EBCM phase function for the oblate spheroid, the parameters for the double H-G function fit for the disc particles could also be found. The EBCM phase functions for oblate spheroids (discs) are similar to those for the prolate spheroids (fibers) to the extent of the comparison to the double H-G function. One can conclude then that these parameters would be not very different from those obtained for the long thin cylinder.

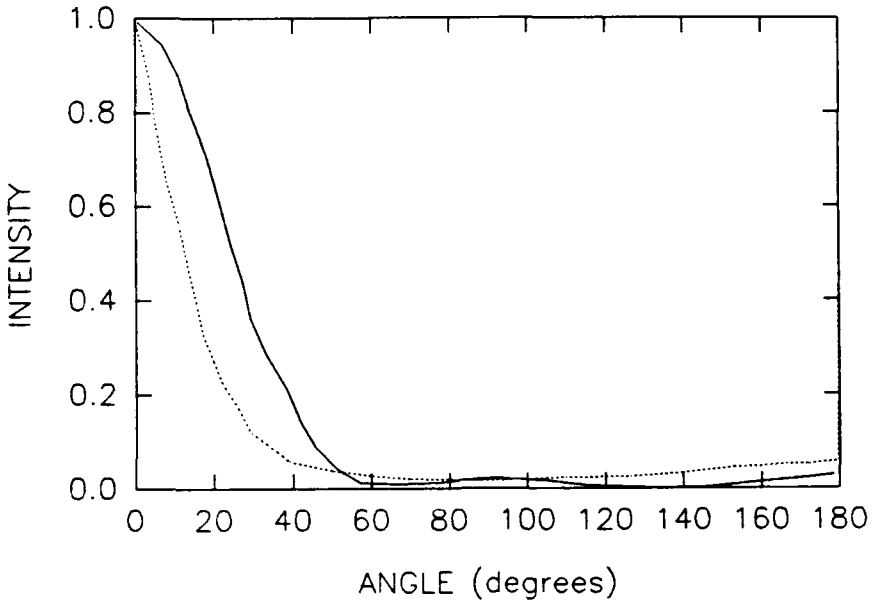

Figure 23. EBCM cylinder - figure 2.7, ka=8.341, $\frac{b}{a}$=0.366 (solid line); H-G phase function with parameters (.75,-.35,.65) (dashed line).

The values found here for g_1, g_2, and β are for the specific data or models that the double H-G phase function was compared to. New double H-G parameters should probably be determined for different cylindrical particles or phase function data. The parameters will be nearly the same for particles of similar size and shape.

5. CONCLUSIONS

One can conclude from this investigation, with the variety of phase functions that are available for cylinders and cylinder-like shapes, that the double H-G phase function can provide a simple, analytic form for the phase function of a cylinder. Exact numerical solutions exist for the infinite cylinder, such as the C-M theory, and these forms for the phase function are useful when numerical solutions are necessary. It is often helpful to have an analytic form for the phase function so that physical intuition can be guided.

An analytic form for the phase function makes the solution to the radiative transfer equations, for example, more tractable as well. When an analytic form for the phase function is available, the equation of transfer and the source function can be written explicitly. It is obvious that if the solution to the equation of transfer exists for the H-G function, it will also exist for the double H-G function. The solution for the double H-G function should be a superposition of the solution for single H-G functions appropriately scaled by the weighting factor. This double H-G phase function is then proposed as an analytic, however approximate, form for the phase function for cylinders. This form is general enough that it can

apply to a variety of cylinder types and sizes.

Recently, a paper was presented at the Annual Transmission Modeling Conference at Hanscom AFB by Cornette (1992). He suggests a similar phase function to the double H-G phase function for use in radiative transfer calculations. Cornette uses a double H-G phase function and does a Lengendre expansion in an attempt to reduce the number of free parameters to 1 and still maintain a good fit to other models.

The major objection to the other analytic forms for the phase function of cylinders discussed in this report is that those forms are for specific cases and types of cylinders. These phase functions do not have the generality that is being sought. In addition, the other phase functions are sometimes computationally intensive to generate. Further work in comparing this double H-G function to actual phase function experimental data and in making radiative transfer calculations with the double H-G function should prove very useful and interesting.

6. ANNOTATED BIBLIOGRAPHY FOR LIGHT SCATTERING BY CYLINDERS

Most of the papers referenced in this report are listed in this annotated bibliography. The annotations are the abstracts that appear with these papers. Pertinent references other than the ones used in this report are listed also.

Asano, S., 1979, "Light Scattering Properties of Spheroidal Particles," *Appl Opt*, 18(5):712-723.

Light scattering characteristics of spheroidal particles are studied for a wide range of particle parameters and orientations. The method of computation is based on the scattering theory for a homogeneous spheroid developed by us, and the calculation is extended to fairly large spheroidal particles of a size parameter up to 30. Effects of the particle size, shape, index of refraction, and orientation on the scattering efficiency factors and the scattering intensity functions are investigated and interpreted physically. The scattering properties of prolate and oblate spheroids with incidence parallel to the rotation axis constitute the extremes. The prolate spheroids with parallel incidence have steep and high-resonance maxima in the scattering efficiency factors and broad and low forward-scattering peaks in the intensity functions; on the other hand, the oblate spheroids at parallel incidence have broad and low resonance maxima and sharp and high forward scattering peaks. With an increase of the incidence angle, the scattering behavior of prolate spheroids approaches that of oblate spheroids at parallel incidence and vice versa. It is shown that, for oblique incidence, the scattering properties of a long, slender prolate spheroid resemble those of an infinitely long cylinder. Effects of absorption on the extinction efficiency factors and the scattering intensity functions are examined. Some problems in numerical calculation of the spheroidal wave functions and the infinite series solution are discussed.

Asano. S., and M. Sato, 1980, "Light Scattering by Randomly Oriented Spheroidal Particles," *Appl Opt*, 19(6):962-974.

Light-scattering properties of an assembly of randomly oriented, identical spheroidal particles are studied. A computation scheme has been developed to integrate the solution of Asano and Yamamoto for scattering from a homogeneous spheroid over all the particle orientations. The extinction and scattering cross sections, asymmetry factor, and scattering matrix elements are calculated for randomly oriented prolate and oblate spheroids and compared with both calculations for spheres and laboratory measurements. The scattering cross section, single-scattering albedo, and asymmetry factor of spheroids tend to be larger than those for spheres of the same volume. The normalized scattering matrix has a symmetrical form with six independent elements. The angular scattering behavior of spheroids is found to be greatly different from that of spheres for side-scattering to back-scattering directions. In general, prolate and oblate spheroids of the same shape parameter have similar scattering patterns.

The angular distribution of scattering intensity is characterized by strong forward scattering and weak back scattering. The linear polarization tends to be positive at intermediate scattering angles. The linear polarization and depolarization are discussed in applications to scattering in the earth and planetary atmospheres.

Asano, S. and G. Yamamoto, 1975, "Light Scattering by a Spheroidal Particle," *Appl Opt*, 14(1):29-49.

The solution of electromagnetic scattering by a homogeneous prolate (or oblate) spheroidal particle with an arbitrary size and refractive index is obtained for any angle of incidence by solving Maxwell's equations under given boundary conditions. The method used is that of separating the vector wave equations in the spheroidal coordinates and expanding them in terms of spheroidal wave functions. The unknown coefficients for the expansion are determined from a system of equations derived from the boundary conditions regarding the continuity of the tangential components of the electric and magnetic vectors across the surface of the spheroid. The solutions in both the prolate and oblate spheroidal coordinate systems result in a same form, and the equations for the oblate spheroidal system can be obtained from those for the prolate one by replacing the prolate spheroidal wave functions with the oblate ones and vice versa. For an oblique incidence, the polarized incident wave is resolved into two components: the TM mode for which the magnetic vector vibrates perpendicularly to the incident plane and the TE mode for which the electric vector vibrates perpendicularly to this plane. For the incidence along the rotation axis, the resultant equations are given in the form similar to the one for a sphere given by Mie theory. The physical parameters involved are the following five quantities: the size parameter defined by the product of semifocal distance of the spheroid and the propagation constant of the incident wave, the eccentricity, the refractive index of the spheroid relative to the surrounding medium, the incident angle between the direction of the incident wave and the rotation axis, and the angles that specify the direction of the scattered wave.

Aquista, C., 1976, "Light Scattering by Tenuous Particles; A Generalization of the Rayleigh-Gans-Rocard Approach," *Appl Opt*, 15(11):2932-2936.

We consider scattering by randomly shaped particles relative to the conditions: (1) that the polarizability of the particle relative to the ambient medium be small compared to 1 and (2) that the phase shift introduced by the particle be less than 2. We solve the integro-differential equation proposed by Shifrin by using the method of successive iterations and then applying a Fourier transform. For the second iteration, results are presented that accurately describe scattering by a broad class of particles. The phase function and other elements of the scattering material are shown to be in excellent agreement with Mie theory for spherical scatterers.

Barber, P. and C. Yeh, 1975, "Scattering of Electromagnetic Waves by Arbitrarily Shaped Dielectric Bodies," *Appl Opt*, 14(12):2864-2872.

The differential scattering characteristics of closed three-dimensional dielectric objects are theoretically investigated. The scattering problem is solved in a spherical basis by the Extended Boundary Condition Method (EBCM) which results in a system of linear equations for the expansion coefficients of the scattered field in terms of the incident field coefficients. The equations are solved numerically for dielectric spheres, spheroids, and finite cylinders to study the dependence of the differential scattering on the size, shape, and index of refraction of the scattering object. The method developed here appears to be most applicable to objects whose physical size is on the order of the wavelength of the incident radiation.

Brillouin, L., 1949, "The Scattering Cross Section of Spheres for Electromagnetic Waves," *J Appl Phys*, 20:1110-1125.

The problem discussed in this paper is that of the scattering of electromagnetic waves by a spherical obstacle. The classical theory is well known. Stratton's "Electromagnetic Theory", for instance, contains a very good summary of that discussion. The computation of the scattering cross section, according to this theory, leads to some difficulties. In the case of large spheres, where geometrical optics should apply, the rigorous theory yields a scattering cross section equal to twice the actual cross section of the sphere!
The discussion presented in this paper explains this strange result and shows the role played by this shadow and by the diffraction fringes surrounding the shadow. A reasonable system of approximations yields the "Babinet's Principle." The physical interpretation is of such a general character that it must certainly apply to a variety of similar problems in acoustics or wave mechanics. The spherical shape of the obstacle is essential in the present discussion, but similar results would certainly be found for other shapes of the obstacle. The case of a circular cylinder, investigated by E. B. Moullin and L. G. Reynolds, also leads to a total cross section twice as large as the actual cross section, for large cylinders. The explanation is the same as for the spheres. Experiments very carefully designed by Dr. Sinclair and Professor V. K. LaMer gave a very precise check of the theoretical predictions.

Bohren, C. F. and D. R. Huffman, 1983, *Absorption and Scattering of Light by Small Particles*, A Wiley-Interscience Publication, John Wiley and Sons.

Part 1, Chapters 1 through 8, is primarily scattering theory. After an introduction there is a chapter on those topics from electromagnetic theory essential to an understanding of the succeeding six chapters on exact and approximate solutions to various scattering problems. Because uninterrupted strings of mathematical formulas tend to pall, computational and experimental results are interspersed throughout these chapters. Bulk matter, rather than particles, is the subject of Part 2. In Chapter 9, we discuss classical theories of optical properties based on idealized models. Such models rarely conform strictly to reality, however, so Chapter 10 presents measurements for three representative materials over a wide range of frequencies from radio to ultraviolet: aluminum, a metal; magnesium oxide, an insulator; and water, a liquid. Part 3 is a marriage of Parts 1 and 2, the offspring of which are chapters on extinction (Chapter 11), surface modes (Chapter 12), and angular scattering (Chapter

13). Applications are not absent from the first thirteen chapters, but there is a greater concentration of them in Chapter 14.

Cheung, R. L-T, and A. Ishimaru, 1982, "Transmission, Backscattering, and Depolarization of Waves in Randomly Distributed Spherical Particles," *Appl Opt*, 21(20):3792-3798.

General formulations are given for the multiple scattering of a polarized wave incident upon a slab of randomly distributed spherical particles. The radiative transfer equation with Stokes vectors is decomposed into Fourier components, and they are shown for linearly and circularly polarized incident wave. For linear polarization, the co-polarized and cross-polarized incoherent intensities show sinusoidal variations with the azimuthal angle. The degree of polarization is also calculated for various directions and optical thickness. The calculations are made for optical waves at 5, 10, and $15\mu m$ in fog and compared with the first order scattering calculations.

Chu, C. M. and H. Weil, 1976, "Integral Equation Method for Scattering and Absorption of Electromagnetic Radiation by Thin Lossy Dielectric Discs," *J Comput Phys* 22:111-124.

An integral equation for the current induced in a dielectric body by incident electromagnetic radiation is solved for the case of a thin flat circular disc of homogeneous lossy dielectric material. The equation is reduced by using the method of moments to a linear algebraic matrix equation for the coefficients in an expansion of the current density as a linear combination of basis functions. The matrix elements consist of integrals involving the basis functions. The novel computational aspects of this work lie in the choice of basis functions and in the techniques which this choice enabled to handle singularities in the integrands when evaluating the matrix elements, to reduce the matrix size and to rigorously preserve the symmetries in the matrix. Expressions are given for the scattering and absorption cross section in terms of the expansion coefficients. The results are most suitable in the resonance range of wavelengths when the disc radius and free-space wavelength are of the same order of magnitude.

Cohen, Ariel, 1980, "Scattering of a Linearly Polarized Incidence at Arbitrary Angle to Incident Plane of Infinite Tilted Cylinder," *Opt Lett* 5(4):150-152.

The general solution of the scattering and extinction of a plane electromagnetic wave by a tilted infinite cylinder is discussed. The scattering equations are extended to the general case with respect to the polarization of the incident light, and it shows that the intensity curves presented previously in the literature for two polarizations (Case I, incident polarization is parallel to the direction of the incident light, and Case II, incident polarization is normal to the incident plane), are not sufficient for the general case. Five relations among the scattering coefficients are presented.

Cohen, Ariel and Charles Aquista, 1982, "Light Scattering by Tilted Cylinders: Properties of Partial Wave Coefficients," *J Opt Soc Am*, 72(5):531-534.

We investigate the relations among the partial-wave coefficients that describe scattering by infinite cylinders in terms of the parameters governing this process: the refractive index m, the size parameter x, the tilting angle θ. We present a complete set of relations for nonabsorbing cylinders, and we discuss the physical significance in terms of the principles of reciprocity and energy conservation. In particular, we find that energy conservation for this nonspherical shape leads to additional constraints not present in the case of scattering by spheres.

Cohen, L. D., R. D. Haracz, A. Cohen, and C. Aquista, 1983, "Scattering of Light From Arbitrarily Oriented Finite Cylinders," *Appl Opt* 22(5):742-748.

An iterative approach to the scattering of light from a finite dielectric cylinder first developed by Shifrin and extended by Aquista is applied to cases where the phase shift is < 2, and the cylinder is arbitrarily oriented. It is found that the first two orders of the iteration converge to within 1% when the aspect ratio (length/diameter) of the cylinder is as small as 20. The results are compared to the exact theory for infinite cylinders, and the effects of finite size are calculated and discussed.

Fowler, B., 1983, "Expansion of Mie-Theory Phase Functions in Series of Legendre Polynomials," *J Opt Soc Am* 73(1).

The method of discrete ordinates in the theory of radiative transfer assumes that the scattering phase functions may be expressed as a series of Legendre polynomials. Previous efforts to calculate the expansion coefficients of these series have been limited to the phase functions of Rayleigh scattering and the unpolarized Mie scattering phase function. In this paper, a methodology for calculating the expansion coefficients of the polarized Mie phase functions is developed as a two-step process. The first step is to develop the computation of the expansion coefficients of the Mie angular amplitudes. These angular amplitude expansion coefficients are then used in the second step to compute the expansion coefficients of the polarized Mie phase functions. Following this, an algorithm suitable for implementing this methodology on a digital computer is developed, and sample calculations are quoted.

Hansen, J. E., and L. D. Travis, 1974, "Light Scattering in Planetary Atmospheres," *Space Science Reviews* 16:527-610.

This paper reviews scattering theory required for analysis of light reflected by planetary atmospheres. Section 1 defines the radiative quantities which are observed. Section 2 demonstrates the dependence of single scattering radiation on the physical properties of the scatters. Section 3 describes several methods to compute the effects of multiple scattering on the reflected light.

Henyey, L. G. and J. L. Greenstein, 1941, "Diffuse Radiation in the Galaxy," *Astrophys J* 93(70).

Observations have been obtained to verify the existence of diffuse stellar radiation. A Fabry photometer attached to the 40-inch refractor at the Yerkes Observatory was used to measure the brightness of regions over a wide range of the galactic latitude. The intensities in the photographic region of the spectrum were calibrated by means of the Polar Sequence stars. The mean of four such runs across the Milky Way, on circles of nearly constant longitude l = 40 degrees, shows a maximum of brightness of 80 stars of the tenth magnitude per square degree for the diffuse extraterrestrial radiation. The mean of three runs at l = 140 degrees shows a maximum of 35 in the same units.
It is shown that the observed intensity of diffuse light may be explained as scattered stellar radiation if the phase function governing the scattering of starlight by the interstellar matter is strongly forward-throwing. The concentration of the diffuse light toward the galactic circle is also in agreement with this property of the phase function. The observations also indicate that the scattering efficiency, or albedo, of the particles is greater than 0.3.

Hering, W. S., 1983, *Analytic Techniques for Estimating Visible Image Transmission Properties of the Atmosphere*, AFGL-TR-83-0236, Hanscom Air Force Base, MA.

The development of field-oriented techniques for determining the atmospheric effects on visible image transmission is described in this report. Simplified analytic methods are presented for calculating the background sky, cloud, and terrain radiance distribution, and in turn the spectral contrast transmittance, of inclined paths of sight in the atmosphere. The directional path radiance is determined as the sum of the singly scattered sunlight component and a multiply-scattered diffuse component that is calculated through application of the delta-Eddington approximation. Performance tests of the model radiance calculations were carried out through comparisons with results from more comprehensive radiative transfer models and by direct comparisons with high resolution scanning radiometer measurements gathered by instrumented aircraft in a broad range of environmental conditions. Techniques for the representation of the optical parameters required as model input data are presented and discussed, including the specification of cloud optical depth as a function of cloud type. An added feature of the contrast transmittance modeling system deals with the combined influences of atmospheric and target factors in order to calculate visual detection range for objects located at the surface and viewed from aloft. Analytic representations of vision experiment data are added along with target information to explore the relative sensitivity of detection range to selected changes in target and atmospheric parameters. Results are presented for several examples assuming simplified targets and backgrounds.

Irving, W. M., 1968, "Multiple Scattering by Large Particles II, Optically Thick Layers," *The Astrophys J* 152:823-834.

Accurate solutions to the scalar equation of transfer in a homogeneous layer with optical thickness $2.5 < T < 8$ are obtained numerically for phase functions with large forward and backward peaks. The Neuman series solution and the doubling method of van de Hulst are employed. The results are presented graphically and are compared with intensities computed

by the small angle method of Romanova and with fluxes computed by Eddington's approximation, the Schuster-Schwarzchild approximation, and modified two-stream approximation. Romanova's method appears quite accurate, but the last three approximations must be used with care for single scattering albedos less than unity.

Irving, W. M., 1975, "Multiple Scattering in Planetary Atmospheres," *Icarus*, 25:175-204.

Methods for solving radiative transfer problems with the extended visible spectrum in planetary atmospheres are reviewed for use by the nonspecialist. Emphasis is placed on rapid, approximate procedures for the determination of such quantities as the plane and spherical (Bond) albedo, surface illumination, absorbed energy, limb darkening, phase curve, and spectra. Precise numerical methods and analytic results are also discussed. Recent approaches to such complications as atmospheric inhomogeneity and reflection from a porous regolith are described briefly.

Ishimaru, A., 1977, "Theory and Application of Wave Propagation and Scattering in Random Media," *Proc IEEE*, 65(7).

This paper presents a review of basic theories and recent advances in the studies of wave propagation and scattering in random media. Examples of the random media include the atmosphere, the ocean, and biological media whose characteristics are randomly varying in time and space. The study of electromagnetic, optical, and acoustic waves in such media has become increasingly important in recent years primarily in the areas of communication, detection, and remote sensing. Topics in this paper are divided into "waves in randomly distributed scatterers", "waves in random continua", and "remote sensing of random media". Transport theory with various approximate solutions and multiple scattering theories are discussed, and their relationships are clarified. Included in the analyses are propagation characteristics of intensities, wave fluctuations, pulse propagation and scattering, coherence bandwidth, and coherence time of communication channels through random media. Remote-sensing techniques include recent advances in the use of inversion techniques to deal with ill-posed problems.

Ishimaru, A., R. L.-T. Cheung, 1980, "Multiple Scattering Effect on Radiometric Determination of Rain Attenuation at Millimeter Wavelengths," *Radio Sci*, 15(3):507-516.

The multiple scattering effects in rain are negligibly small in comparison with the absorption effects when raindrop sizes are much smaller than the wavelength. This is often true for light to moderate rain below 30 GHz, and the total atmospheric attenuation along the path may be estimated by the emission method using the usual radiometric formula. At higher frequencies and in heavy rain, the multiple scattering effects cannot be ignored. This paper describes a theoretical study of the correction due to the multiple scattering effect for the determination of the total atmospheric attenuation by the emission method. The observed temperatures at the ground, both for vertical and horizontal polarizations and for various raindrop temperatures, precipitation rates, ground temperatures, ground albedos,

and frequencies ranging from 30 GHz to 120 GHz are calculated on the basis of the equation of transfer, taking into account the polarizations and the Stokes parameters. The cross sections of rain droplets are calculated using the Mie solution with the Laws and Parsons drop size distribution and Saxon's formula for the refractive index of water. These calculations show the differences between the total rain attenuation and the attenuation calculated from the sky temperature measurements and the assumed rain temperatures. The results are compared to some experimental data, showing good agreement.

Ishimaru, A., D. Lesselier, and C. Yeh, 1984, "Multiple Scattering Calculations for Nonspherical Particles Based on the Vector Radiative Transfer Theory," *Radio Science*, 19(5):1356-1366.

On the basis of the vector radiative transfer equation, multiple scattering calculations were performed for an obliquely incident linearly polarized plane wave upon a plane parallel slab consisting of arrays of vertically oriented, uniformly distributed nonspherical spheroidal particles of identical size. Results are given in terms of the Stokes parameters for the incoherent field. Owing to the symmetry of the particles and their orientation, decoupling of the Fourier expansion coefficients in the solution of the radiative transfer equation occurs. Each Fourier component satisfies a single equation which is then solved by Gauss's quadrature and the eigenvalue-eigenvector technique. The behavior of the forward scattered incoherent field is investigated for low-loss as well as high-loss particles, for different densities and shapes, and for various angles of incidence. Comparisons of the results from the approximate first-order theory shows good quantitative agreement for thin and sparsely populated layers.

Ishimaru, A., R. Woo, J. W. Armstrong, and D. C. Blackman, 1982, "Multiple Scattering Calculations of Rain Effects," *Radio Science*, 17(6):1425-1433.

At millimeter wave frequencies, the scattering cross section of raindrops becomes comparable to the absorption cross section, and incoherent intensity due to multiple scattering may become significant. This paper presents calculations of the incoherent intensity at 30, 60, 90, and 120 GHz. The scattering and absorption characteristics of the rain are calculated using the Mie solution and the Laws-Parsons distribution. Incoherent intensities for the horizontal and vertical polarizations are obtained using the equation of transfer and the Stokes parameters. The obliquely incident wave is linearly polarized. The equation of transfer is solved using the Gauss quadrature formula and the matrix eigenvalue technique. The matrix elements are calculated using the formulations developed by Sekera, and the vertical and horizontal components and their correlations are used in the Stokes parameter representations. The received incoherent intensity depends on the field of view of the receiving antenna. The ratio of the co-polarized incoherent intensity to the polarized component is defined as the incoherent co-polarized discrimination I-CPD, and the ratio of the cross-polarized incoherent intensity to the co-polarized coherent intensity is defined as the incoherent cross-polarized discrimination I-XPD. These are computed in terms of rain rate, field of view, and co-polarized attenuation. It is shown that multiple scattering effects may

become significant during heavy rains. Back scattering results are also presented.

Ishimaru, A., and C. W. Yeh, 1984, "Matrix Representations of the Vector Radiative-Transfer Theory for Randomly Distributed Nonspherical Particles," *J Opt Soc Am A*, 1(4):359-364.

General matrix representation of the vector radiative-transfer equation for randomly distributed nonspherical particles is given with compact representations of the extinction matrix and the Mueller matrix. The propagation of the coherent Stokes vector and the coherency matrix in such a medium is expressed in matrix form. The extinction matrix is related to the generalized optical theorem for partially polarized waves. The first-order scattering solution of the Stokes vector is given in matrix form, and discussion of the Fourier expansion of the equation of transfer and the limitation of the equation of transfer are given.

Ishimaru, A., C. Yeh, and D. Lesselier, 1984, "First-Order Multiple Scattering Theory for Nonspherical Particles," *Appl Opt*, 23(22):4132-4139.

Using the vector radiative transfer equation, we have obtained the first-order solution for the problem dealing with multiple scattering from an ensemble of nonspherical particles. Representative results for low-absorbent disks (oblate spheroids) as well as high-absorbent disks were obtained. In general, it was found that multiple scattering effects were more prominent for the low-absorbent particles.

Joseph, J. H., W. J. Wiscombe, and J. A. Weinman, 1976, "The Delta-Eddington Approximation for Radiative Flux Transfer," *Jour Atmos Sci*, 33:2452-2459.

This paper presents a rapid yet accurate method, the "delta-Eddington" approximation, for calculating monochromatic radiative fluxes in an absorbing-scattering atmosphere. By combining a Dirac delta function and a two-term approximation, it overcomes the poor accuracy of the Eddington approximation for highly asymmetric phase functions. The fraction of scattering into the truncated forward peak is taken as proportional to the square of the phase function asymmetry factor, which distinguishes the delta-Eddington approximation from others of a similar nature. Comparison of delta-Eddington albedos, transmissivities, and absorbtivities with more exact calculations reveal typical differences of 0-0.02 and maximum differences of 0.15 over wide ranges of optical depth, sun angle, surface albedo, single-scattering albedo, and phase function asymmetry factor. Delta-Eddington fluxes are in error, on the average, by no more than 0.5%, and at the maximum by no more of 2% of the incident flux. This computationally fast and accurate approximation is potentially of utility in applications such as general circulation and climate modeling.

Kattawar, G. W., 1975, "A Three-Parameter Analytic Phase Function for Multiple Scattering Calculations," *J Quant Spectros Radiat Trans*, 15:839-849.

A very simple procedure has been developed to fit the first three moments of an actual phase function with a three-parameter analytic phase function. The exact Legendre polynomial

decomposition of this function is known which makes it quite suitable for multiple scattering calculations. The use of this function can be expected to yield excellent flux values at all depths within a medium. Since it is capable of reproducing the glory, it can be used in synthetic spectra computations from planetary atmospheres. Accurate asymptotic radiance values can also be achieved as long as the single scattering albedo w$\geq$0.9.

Liou, K. N., 1972, "Electromagnetic Scattering by Arbitrarily Oriented Ice Cylinders," *Appl Opt*, 11(?):667-674.

The scattering of electromagnetic waves by arbitrarily oriented, infinitely long circular cylinders is solved by following the procedures outlined by van de Hulst. The far-field intensities for two cases of a linearly polarized incident wave are derived. The scattering coefficients involve the Bessel functions of the first kind, the Hankel functions of the second kind, and their first derivatives. Calculations are made for ice cylinders at three wavelengths: 0.7μm, 3μm, and 10μm. The numerical results of intensity coefficients are presented as functions of the observation angle θ. A significant cross-polarized component for the scattered field, which vanishes only at normal incidence, is obtained. It is also shown that the numerous interference maxima and minima of the intensity coefficients due to single particle effects depend on the size parameter x as well as on the oblique incidence angle α. Since cylinder-type particles are often observed in ice clouds, the light scattering calculations performed for a circular cylinder in this paper should be of use in the study of cloud microstructure.

Liou, K. N., 1972, "Light Scattering by Ice Clouds in the Visible and Infrared: A Theoretical Study," *J Atmos Sci*, 29:524-536.

Computations of the intensity and linear polarization for single scattering by ice clouds have been made based on the assumption that the particles in ice clouds can be approximated by long circular cylinders which are allowed to be polydispersive as well as arbitrarily oriented in space. The results of two models of optically thin ice clouds are presented and compared with those for polydisperse ice spheres. The two models for ice cylinders are assumed to be either uniformly or randomly oriented in a horizontal plane. Four different wavelengths, 0.7, 3, 3.5, and 6.05 μm, are employed in the light scattering computations.
It is found that, compared to ice spheres, long ice cylinders scatter more light in the region with scattering angles near 90 degrees, at the expense of scattering in both the forward and backward directions. The glory and cloudbows, which occur in light scattered by spherical particles, are either lost (the glory) or largely reduced or distorted (the cloudbows) in the case of cylinders. It is probable that for more irregular particles the cloudbows would also disappear. These differences in scattering by spherical and nonspherical scatterers therefore provide useful information for the differentiation between the ice and liquid phases of cloud particles.
The light scattering computations performed for ice cylinders in this paper represent a new theoretical approach in an attempt to understand the radiation scattered by ice crystals. Hence, results of the angular scattering patterns for ice cylinders could be of use in the

evaluation of the transfer of visible or infrared radiation through thick ice clouds especially cirrus.

Mott, D. L. and D. R. Brown, 1983, *EBCM Program: User's Guide*, CR-84-0009-3, U.S. Army Electronics Research and Development Command Contractor Technical Report.

Information in the use of a family of extended boundary condition method (EBCM) programs is provided for the calculation of scattering by nonspherical, rotationally symmetric particles. The individual FORTRAN programs are described, listings given, and sample runs provided. An additional note is made here by the compilers of this annotated bibliography. The FORTRAN code for the EBCM has been dumped onto the HP9000 system but has not been converted for use there. The extent of the problem of conversion has not been evaluated but superficially appears to be a significant problem. The EBCM code was developed for Mott and Brown by James Pratt of PSL on the New Mexico State University Amdahl computer system. The code was used extensively on that system, so any problems in use of the code (other than convergence problems) will be concerned with computer conversion problems.

Pedersen, N. E., J. C. Pedersen, and P. C. Waterman, 1985, *Final Report on Theoretical Study of Single and Multiple Scattering by Cylinders*, CRDC-CR-85014.

Closed-form analytic results are obtained for the calculation of the electromagnetic differential and total scattering, absorption, and extinction cross sections of arbitrarily oriented conductive fibers. An extensive computer program has been developed for the computation of these quantities. The results agree with expectations for arbitrary conductivity, arbitrary length-to-wavelength ratio, and radius-to-wavelength ratio less than 0.3. Two minor exceptions are noted and discussed. The albedo of the particle is computed as are the appropriately averaged differential scattering cross sections. These quantities serve as inputs to a Radiative Transfer computer program which was developed concurrently to calculate and plot the angular distributions of reflected and transmitted radiation from large aggregates of the particles.

Reynolds, L. O. and N. J. McCormick, 1980, "Approximate Two-Parameter Phase Function for Light Scattering," *J Op Soc Am*, 70(10).

A two-parameter phase function is described for highly anisotropic angular scattering distributions. The phase function has a convenient analytic representation since it is the generating function for the Gegenbauer (or ultraspherical) polynomials. Simple calculations illustrate the large variety of forward-to-backward scattering amplitudes and shapes that can be fit with the two parameters. Illustrative phase functions are given that approximate light scattering distributions predicted for several biological and atmospheric specimens from Rayleigh-Gans and Mie models. A suggested classification scheme for size and refractive index of microparticles in human blood is presented as a potential application of the phase function with two parameters.

Senior, T. B. A. and H. Weil, 1977, "Electromagnetic Scattering and Absorption by Thin Walled Dielectric Cylinders With Applications to Ice Crystals," *Appl Opt*, 16(11):2979-2985.

Integral equations are developed to determine the scattering and absorption of electromagnetic radiation by thin walled cylinders of arbitrary cross section and refractive index. Numerical data are presented at wavelengths in the ir for hollow, circular, and hexagonal cross-section cylinders which simulate columnar sheath ice crystals. The numerical procedures are economical for cylinders whose perimeters are less than about fifteen free-space wavelengths.

Strom, S., 1975, "On the Integral Equations for Electromagnetic Scattering," *Am J Phys*, 43(12):1060-1069.

In the present article, we discuss several volume and surface integral expressions for an electromagnetic field in the presence of a scatterer of finite extension, with special emphasis on a description of the scattering by means of a transition matrix.

Stroud, D., 1976, "Generalized Effective Medium Approach to the Conductivity of an Inhomogeneous Material," *Phys Rev B*, 12(8):3368-3373.

An old effective-medium approximation for the conductivity tensor of a randomly inhomogeneous medium is generalized to treat, in principle, materials consisting of crystallites of arbitrary shape and conductivity tensors of arbitrary symmetry. The effective medium approximation is roughly analogous to the coherent potential approximation (CPA) of alloy theory. The analog of the average-t-matrix approximation (ATA) is also formulated in a general way. The method is fully tractable analytically for ellipsoidal crystallites. Several applications are discussed. The effective conductivity of a polycrystal consisting of randomly oriented uniaxial crystallites is calculated as a function of the anisotropy of the grains. For a model polycrystal in an intense magnetic field, the CPA and ATA are compared, the former giving more accurate results.

van de Hulst, H. S., 1981, *Light Scattering by Small Particles*, Dover Publications, (J. Wiley and Sons, Inc. 1957).

This book is divided into three sections: Basic Scattering Theory, Special Types of Particles, and Applications. The Basic Scattering Theory covers five chapters: an introduction, conversation of energy and momentum, wave propagation in vacuum, wave propagation in a medium containing scatters, and polarized light and symmetry relations. There are twelve chapters in the second section. They are particles small compared to the wavelength, Rayleigh-Gans scattering, particles very large compared to the wavelength, rigorous scattering theory for spheres of arbitrary size (Mie theory), nonabsorbing spheres, spheres with refractive index near 1, very large spheres, optics of a rainbow, absorbing spheres, circular cylinders, particles of other forms, and edge phenomena and surface waves. The last section contains four chapters; scattering and extinction experiments as a tool, applications to chemistry, applications to meteorology, and applications to astronomy.

Weil, H., and C. M. Chu, 1976, "Scattering and Absorption of Electromagnetic Radiation by Thin Dielectric Disks," *Appl Opt*, 15(7):1832-1836.

The scattering and absorption of incident polarized radiation by thin flat circular disks composed of homogeneous isotropic material of complex refractive index are investigated by solving an integral equation for the induced currents. The method is particularly suitable for use in the resonant region where the free space wavelength is neither very small nor very large compared to the radius. Illustrative numerical results for bi-static, total, and absorption cross sections for broadside and edge-on incidence are given, using refractive indices for ice in the ir.

References

Barber, P. and C. Yeh, 1975, "Scattering of Electromagnetic Waves by Arbitrarily Shaped Dielectric Bodies," *Appl Opt*, 14(12):2864-2872.

Bohren, C. F. and D. R. Huffman, 1983, *Absorption and Scattering of Light by Small Particles*, A Wiley-Interscience Publication, John Wiley and Sons.

Cornette, William M., 1992, "A Physically Reasonable Analytic Expression for the Single Scattering Phase Function", *Proceedings of the Annual Transmission Modeling Meeting*, Hanscom AFB. This paper has also been accepted for publication and will be published in Applied Optics in 1992.

Gillespie, James B., and George H. Goedecke, 1989, "Refractive Indices of Powdered Materials Using Attenuated Total Reflectance Spectroscopy", *Appl Opt*, 28(18):3985-3992.

Henyey, L. G. and J. L. Greenstein, 1941, "Diffuse Radiation in the Galaxy," *Astrophys J*, 93(70).

Ishimaru, A., 1977, "Theory and Application of Wave Propagation and Scattering in Random Media," *Proc IEEE*, 65(7).

Kattawar, G. W., 1975, "A Three-Parameter Analytic Phase Function for Multiple Scattering Calculations," *J Quant Spectros Radiat Trans*, 15:839-849.

Mott, D. L. and D. R. Brown, 1984, "EBCM Program: User's Guide," CR-84-0009-3, U. S. Army Electronics Research and Development Command Contractor Technical Report.

Reynolds, L. O. and N. J. McCormick, 1980, "Approximate Two-Parameter Phase Function for Light Scattering," *J Op Soc Am*, 70(10).

van de Hulst, H. S., 1957, *Light Scattering by Small Particles*, Dover Publications, J. Wiley and Sons, Inc. 1957.

DISTRIBUTION LIST FOR PUBLIC RELEASE

Commandant
U.S. Army Chemical School
ATTN: ATZN-CM-CC (S. Barnes)
Fort McClellan, AL 36205-5020

Commander
U.S. Army Aviation Center
ATTN: ATZQ-D-MA
Mr. Oliver N. Heath
Fort Rucker, AL 36362

NASA/Marshall Space Flight Center
Deputy Director
Space Science Laboratory
Atmospheric Sciences Division
ATTN: E501 (Dr. George H. Fichtl)
Huntsville, AL 35802

NASA/Marshall Space Flight Center
Atmospheric Sciences Division
ATTN: Code ED-41
Huntsville, AL 35812

Deputy Commander
U.S. Army Strategic Defense Command
ATTN: CSSD-SL-L
Dr. Julius Q. Lilly
P.O. Box 1500
Huntsville, AL 35807-3801

Commander
U.S. Army Missile Command
ATTN: AMSMI-RD-AC-AD
Donald R. Peterson
Redstone Arsenal, AL 35898-5242

Commander
U.S. Army Missile Command
ATTN: AMSMI-RD-AS-SS
Huey F. Anderson
Redstone Arsenal, AL 35898-5253

Commander
U.S. Army Missile Command
ATTN: AMSMI-RD-AS-SS
B. Williams
Redstone Arsenal, AL 35898-5253

Commander
U.S. Army Missile Command
ATTN: AMSMI-RD-DE-SE
Gordon Lill, Jr.
Redstone Arsenal, AL 35898-5245

Commander
U.S. Army Missile Command
Redstone Scientific Information
Center
ATTN: AMSMI-RD-CS-R/Documents
Redstone, Arsenal, AL 35898-5241

Commander
U.S. Army Intelligence Center
and Fort Huachuca
ATTN: ATSI-CDC-C (Mr. Colanto)
Fort Huachuca, AZ 85613-7000

Northrup Corporation
Electronics Systems Division
ATTN: Dr. Richard D. Tooley
2301 West 120th Street, Box 5032
Hawthorne, CA 90251-5032

Commander - Code 3331
Naval Weapons Center
ATTN: Dr. Alexis Shlanta
China Lake, CA 93555

Commander
Pacific Missile Test Center
Geophysics Division
ATTN: Code 3250 (Terry E. Battalino)
Point Mugu, CA 93042-5000

Lockheed Missiles & Space Co., Inc.
Kenneth R. Hardy
Org/91-01 B/255
3251 Hanover Street
Palo Alto, CA 94304-1191

Commander
Naval Ocean Systems Center
ATTN: Code 54 (Dr. Juergen Richter)
San Diego, CA 92152-5000

Meteorologist in Charge
Kwajalein Missile Range
P.O. Box 67
APO San Francisco, CA 96555

U.S. Department of Commerce
Mountain Administration Support
Center
Library, R-51 Technical Reports
325 S. Broadway
Boulder, CO 80303

Dr. Hans J. Liebe
NTIA/ITS S 3
325 S. Broadway
Boulder, CO 80303

NCAR Library Serials
National Center for Atmos Rsch
P.O. Box 3000
Boulder, CO 80307-3000

HQDA
ATTN: DAMI-POI
Washington, D.C. 20310-1067

Mil Asst for Env Sci Ofc of
The Undersecretary of Defense
for Rsch & Engr/R&AT/E&LS
Pentagon - Room 3D129
Washington, D.C. 20301-3080

Director
Naval Research Laboratory
ATTN: Code 4110
Dr. Lothar H. Ruhnke
Washington, D.C. 20375-5000

HQDA
DEAN-RMD/Dr. Gomez
Washington, D.C. 20314

Director
Division of Atmospheric Science
National Science Foundation
ATTN: Dr. Eugene W. Bierly
1800 G. Street, N.W.
Washington, D.C. 20550

Commander
Space & Naval Warfare System Command
ATTN: PMW-145-1G (LT Painter)
Washington, D.C. 20362-5100

Commandant
U.S. Army Infantry
ATTN: ATSH-CD-CS-OR
Dr. E. Dutoit
Fort Benning, GA 30905-5090

USAFETAC/DNE
Scott AFB, IL 62225

Air Weather Service
Technical Library - FL4414
Scott AFB, IL 62225-5458

HQ AWS/DOO
Scott AFB, IL 62225-5008

USAFETAC/DNE
ATTN: Mr. Charles Glauber
Scott AFB, IL 62225-5008

Commander
U.S. Army Combined Arms Combat
ATTN: ATZL-CAW (LTC A. Kyle)
Fort Leavenworth, KS 66027-5300

Commander
U.S. Army Space Institute
ATTN: ATZI-SI (Maj Koepsell)
Fort Leavenworth, KS 66027-5300

Commander
U.S. Army Space Institute
ATTN: ATZL-SI-D
Fort Leavenworth, KS 66027-7300

Commander
Phillips Lab
ATTN: PL/LYP (Mr. Chisholm)
Hanscom AFB, MA 01731-5000

Director
Atmospheric Sciences Division
Geophysics Directorate
Phillips Lab
ATTN: Dr. Robert A. McClatchey
Hanscom AFB, MA 01731-5000

Raytheon Company
Dr. Charles M. Sonnenschein
Equipment Division
528 Boston Post Road
Sudbury, MA 01776
Mail Stop 1K9

Director
U.S. Army Materiel Systems
Analysis Activity
ATTN: AMXSY-MP (H. Cohen)
APG, MD 21005-5071

Commander
U.S. Army Chemical Rsch,
Dev & Engr Center
ATTN: SMCCR-OPA (Ronald Pennsyle)
APG, MD 21010-5423

Commander
U.S. Army Chemical Rsch,
Dev & Engr Center
ATTN: SMCCR-RS (Mr. Joseph Vervier)
APG, MD 21010-5423

Commander
U.S. Army Chemical Rsch,
Dev & Engr Center
ATTN: SMCCR-MUC (Mr. A. Van De Wal)
APG, MD 21010-5423

Director
U.S. Army Materiel Systems
Analysis Activity
ATTN: AMXSY-AT (Mr. Fred Campbell)
APG, MD 21005-5071

Director
U.S. Army Materiel Systems
Analysis Activity
ATTN: AMXSY-CR (Robert N. Marchetti)
APG, MD 21005-5071

Director
U.S. Army Materiel Systems
Analysis Activity
ATTN: AMXSY-CS (Mr. Brad W. Bradley)
APG, MD 21005-5071

Commander
U.S. Army Laboratory Command
ATTN: AMSLC-CG
2800 Powder Mill Road
Adelphi, MD 20783-1145

Commander
Headquarters
U.S. Army Laboratory Command
ATTN: AMSLC-CT
2800 Powder Mill Road
Adelphi, MD 20783-1145

Commander
Harry Diamond Laboratories
ATTN: SLCIS-CO
2800 Powder Mill Road
Adelphi, MD 20783-1197

Director
Harry Diamond Laboratories
ATTN: SLCHD-ST-SP
Dr. Z.G. Sztankay
Adelphi, MD 20783-1197

National Security Agency
ATTN: W21 (Dr. Longbothum)
9800 Savage Road
Ft George G. Meade, MD 20755-6000

U. S. Army Space Technology
and Research Office
ATTN: Brenda Brathwaite
5321 Riggs Road
Gaithersburg, MD 20882

OIC-NAVSWC
Technical Library (Code E-232)
Silver Springs, MD 20903-5000

The Environmental Research
Institute of MI
ATTN: IRIA Library
P.O. Box 134001
Ann Arbor, MI 48113-4001

Commander
U.S. Army Research Office
ATTN: DRXRO-GS (Dr. W.A. Flood)
P.O. Box 12211
Research Trianagle Park, NC 27709

Dr. Jerry Davis
North Carolina State University
Department of Marine, Earth, &
Atmospheric Sciences
P.O. Box 8208
Raleigh, NC 27650-8208

Commander
U. S. Army CECRL
ATTN: CECRL-RG (Dr. H. S. Boyne)
Hanover, NH 03755-1290

Commanding Officer
U.S. Army ARDEC
ATTN: SMCAR-IMI-I, Bldg 59
Dover, NJ 07806-5000

U.S. Army Communications-Electronics
Command Center for EW/RSTA
ATTN: AMSEL-RD-EW-SP
Fort Monmouth, NJ 07703-5303

Commander
U.S. Army Communications-Electronics
Command
ATTN: AMSEL-EW-D (File Copy)
Fort Monmouth, NJ 07703-5303

Headquarters
U.S. Army Communications-Electronics
Command
ATTN: AMSEL-EW-MD
Fort Monmouth, NJ 07703-5303

Commander
U.S. Army Satellite Comm Agency
ATTN: DRCPM-SC-3
Fort Monmouth, NJ 07703-5303

Director
EW/RSTA Center
ATTN: AMSEL-EW-DR
Fort Monmouth, NJ 07703-5303

USACECOM
Center for EW/RSTA
ATTN: AMSEL-RD-EW-SP
Fort Monmouth, NJ 07703-5303

6585th TG (AFSC)
ATTN: RX (CPT Stein)
Holloman AFB, NM 88330

Department of the Air Force
OL/A 2nd Weather Squadron (MAC)
Holloman AFB, NM 88330-5000

PL/WE
Kirtland AFB, NM 87118-6008

Director
U.S. Army TRADOC Analysis Command
ATTN: ATRC-WSS-R
White Sands Missile Range, NM 88002

Rome Laboratory
ATTN: Technical Library RL/DOVL
Griffiss AFB, NY 13441-5700

Department of the Air Force
7th Squadron
APO, NY 09403

AWS
USAREUR/AEAWX
APO, NY 09403-5000

AFMC/DOW
Wright-Patterson AFB, OH 0334-5000

Commander
U.S. Army Field Artillery School
ATTN: ATSF-F-FD (Mr. Gullion)
Fort Sill, OK 73503-5600

Commandant
U.S. Army Field Artillery School
ATTN: ATSF-TSM-TA
Mr. Charles Taylor
Fort Sill, OK 73503-5600

Commander
Naval Air Development Center
ATTN: Al Salik (Code 5012)
Warminister, PA 18974

Commander
U.S. Army Dugway Proving Ground
ATTN: STEDP-MT-DA-M
Mr. Paul Carlson
Dugway, UT 84022

Commander
U.S. Army Dugway Proving Ground
ATTN: STEDP-MT-DA-L
Dugway, UT 84022

Commander
U.S. Army Dugway Proving Ground
ATTN: STEDP-MT-M (Mr. Bowers)
Dugway, UT 84022-5000

Defense Technical Information Center
ATTN: DTIC-FDAC
Cameron Station
Alexandria, VA 22314

Commanding Officer
U.S. Army Foreign Science &
Technology Center
ATTN: CM
220 7th Street, NE
Charlottesville, VA 22901-5396

Naval Surface Weapons Center
Code G63
Dahlgren, VA 22448-5000

Commander
U.S. Army OEC
ATTN: CSTE-EFS
Park Center IV
4501 Ford Ave
Alexandria, VA 22302-1458

Commander and Director
U.S. Army Corps of Engineers
Engineer Topographics Laboratory
ATTN: ETL-GS-LB
Fort Belvoir, VA 22060

TAC/DOWP
Langley AFB, VA 23665-5524

U.S. Army Topo Engineering Center
ATTN: CETEC-ZC
Fort Belvoir, VA 22060-5546

Commander
Logistics Center
ATTN: ATCL-CE
Fort Lee, VA 23801-6000

Commander
USATRADOC
ATTN: ATCD-FA
Fort Monroe, VA 23651-5170

Science and Technology
101 Research Drive
Hampton, VA 23666-1340

Commander
U.S. Army Nuclear & Cml Agency
ATTN: MONA-ZB Bldg 2073
Springfield, VA 22150-3198